Reply to referees:

First thing first, we would like to thank the referees for their work and valuable comments. Based on their comments, we believe we have significantly changed and improved the manuscript. The revised version was attached after the replies.

Before we go to the detailed replies, we need to clarify the structure revision. Our idea for this paper are twofold. First, we used the daytime MICROTOPS II data and nighttime lidar data to validate the shipborne CE318-T, which is never done before. In this case, we found results of the shipborne CE318-T are convincing and its setup is robust to enable continuous and unattended measurements over the harsh maritime environment. This is a great benefit for future MOSAiC campaign, because it will on-board RV *Polarstern* again and join the 1 year Arctic measurement campaign, which was dedicated to address our human effects for climate change. On the other hand, we used the shipborne CE318-T data to facilitate the lidar data analysis, for instance, using the AOD measurements from the sunphotometer to constrain the Fernald retrieval for dust cases in Sect 3.2.2, using the Angstroem exponent for Raman retrieval to calculate the vertical aerosol extinction coefficient profile and also using the integrated water vapor to calibrate the lidar water vapor channel to retrieve the vertical water vapor mixing ratio (this part was not included in the paper). These are of great importance to enable operational lidar data analysis for future OCEANET and MOSAiC campaigns as well. We hope with these structure changes, we make the highlights clear.

Besides, we want to correct our descriptions about MICROTOPS II configurations. In the original version, we **made a mistake about the channels, which stated there was a channel at 500 nm**. But after our checking for the manual, **we found there was no 500 nm channel inside**. The AOD at this wavelength from MAN was interpolated with using the Ångström exponent. Therefore, we need to correct this in Sect 2.2. But this correction didn't have influences on the conclusions we've drawn before, because we added the AOD comparisons with other wavelengths at this time and also found good agreement.

Item by item response to the comments of the reviewers, (comments are in bold)

Response to Anonymous Referee #1

…, but am struggling to understand the direction of the paper. Is this intended to be a validation of the sun photometer observations? If so, I find this to be an overly superficial analysis that does not make the case that this instrument is ready for adoption yet. Is this intended to be an examination of the aerosol state in Atlantic transects? If so, I'm not sure what new information is being presented, nor the implications for our knowledge of the atmosphere.

Author response (AR): We feel sorry for the confusing message delivered by this article, and we have revised the structure according to your comments (see the beginning). The motivation for this paper is to validate the shipborne sunphotometer with collocated MICROTOPS II and lidar, and shows its potential for regular lidar data analysis.

Regarding the validation analysis, we revised the whole part with Bland-Altman plot and added more details as being suggested. Detailed replies can be found below and the revisions can be found in the new Sect 3.1 (highlight with color red).

… 1. How different is the shipborne CE318-T from the standard (land based model)? I see that an air pump has been added, along with an anemometer and compass. But how are the compass and GPS data used to help the instrument track the sun? Compensating for ship motion has been an engineering challenge for such instruments for quite sometime, so a description of how this has been solved is needed. 2. Does the instrument have a different measurement protocol than the CE318-T? Does it require special data processing? What are the limits of its operation? The anemometer is presumably intended to determine the wind speed and park the instrument when it becomes too rough – at what wind speed does this occur? 3. How accurate do you expect the instrument to be?

AR: The instrument is an extended version of land-based CE318-T. The optical head, GPS and rotation base is still the same. But we added additional air-flow system, compass and anemometer to deal with the harsh maritime environment. The SUN and MOON measurements are still the same but we inserted the GPS data to each line of AOD data. Therefore, each AOD data has a dynamic position tag, compared with the static coordinate for land-based model. That makes the data processing a little bit different, because the additional GPS infomation must be included. At present, this data structure is only incorporated in the PHOTONS database.

For the weather stop system and limits of its operation, we only took into account of rain and wind. For the rain detection, we changed the basic wet sensor (a resistor) for land-based CE318-T with an optical rain sensor. Because the former one didn't work well under the sea conditions due to the corrosion from sea salt. For the limit of wind speed, we set it to be 40 km/h, which is an arbitrary choice. However, this value must be smaller than 45 km/h. Because at that level, as we tested, the robot head will be vibrated by the wind (We can also see this effect in the data).

For the accuracy, we expected it like the AERONET data because the final triplet, including the cloud screening, is the same like AERONET.

Some of the changes regarding this comment was also added in Sect. 2.1 (in red)

I would assume calibration and shot noise errors are identical to the land based version, but is there an additional error source due to the difficulties of sun tracking?

AR: Yes, it's possible for the additional error source from the sun tracking, if the ship moves too fast or the wind is too strong. But under that conditions, the upgraded tracking system can compensate large part of the movements and

vibrations. Besides, the triplet check will help filter the data with large variability over 30 s as well. These can screen out measurements under unstable sun tracking due to the vibrations of optical head and tracking base. If there were still possibility for bad data coming from failed sun tracking, we still have additional data from GPS and anemometer to help us exclude the results. And through the comparisons with MICROTOPS, we do see good agreement without any further data quality control.

These issues would be less relevant if there were some prior literature describing them. As far as I can tell, the only potential description is in the Goloub citation which is a slide presentation for me not appropriate for use as a reference. In any case, that document does not resolve the questions I noted previously. So it falls to this publication to make these things clear.

AR: More technical details (in red) about the shipborne CE318-T were added in Sect. 2.1, which was listed as below,

"The optical head was the same like the other land-based CE318-T. The GPS and compass modules (SIMRAD HS60) were fixed on the platform together with the photometer robot to assure the same motions. In order to track the sun continuously over the ship, the photometer will firstly go to the sun with the last information (date, time, geolocation, heading, pitch and roll) from the GPS and compass modules. This can help the photometer point to the sun if the ship does not turn quickly. If it does not see the sun, which can be determined through the digital number from direct sun measurements, the head will be controlled to search the sky at 45^0 in left and right horizontal panel of its first position. When it detects the sun, the new position will be used to calculate the turning angle of the ship and then to correct the azimuth position for the next measurements. When the sun is in the tracking field of view (~ 10^0), the photometer will switch into tracking mode like a regular photometer. But unlike a conventional CE318-T, the tracking mode by using the 4-quadrant detector, will keep working to compensate the motions of the ship during all the SUN triplet measurements. And for moon triplet measurements, it's also the same procedure. Because of the same triplets. The air pumping module generates compressed dry-clean air to the collimator to prohibit the contamination of optical window by ambient sea spray. Meanwhile, we changed the wet sensor by an optical rain sensor to prevent the influence of the strong corrosion from the sea spray. And we also added an anemometer to help us stop the system, because the robot itself will vibrate as wind speed over 45 km/h. We arbitrarily chose the limit of 40 km/h for our measurements."

… Section 3.2.3: an interesting idea to compare this, but I find it very difficult to follow. It is not even clear which data (or times) are associated with day and night – I have to guess based on the blackout time near solar noon in the lidar data.

AR: Thanks for pointing out this. For the new version, we added vertical lines and marks with black color about the sunrise and sunset in Figure 6

The conclusions mention issues in this comparison and sensitivity to leveling errors in night time data. But I see no description of these problems in the actual section the conclusion refers to! The conclusion must be supported by previous sections, it is not a place to reveal new information.

AR: We fully agree. It is also too early to draw this conclusion because there are many factors which can contribute to the uncertainty of nighttime measurements, for instance, the weak moon illumination, leveling error and large ship turnings during the night. Based on our measurements, we cannot see which one contributed the most. Therefore, we decided to remove this conclusion.

Section 3.2: it is unfortunately common in analysis today, but the use of linear regressions and the coefficient of determination to test the hypothesis that two types of measurements agree is statistically unsound. This is especially the case for AOD, which tends to have a log-normal distribution, not a normal distribution that is the basis for linear regression statistics…

AR: This is a very valuable comment! Triggered by this, we have redone the statistical analysis about the measurement agreements between CE318-T and MICROTOPS II in Sect. 3.1 for the wavelengths of 380, 440, 500 and 870 nm, which was shared by the two instruments. Besides, as suggested, we added the Bland-Altman plot in Figure 5.

Our procedures for the analysis followed 3.C in (Knobelspiesse et al., 2019) and we only use the AOD between 0.04 and 0.2, according to traceability requirements stated in (WMO). This also helps to narrow down the aerosol features to mainly marine aerosols. Our results showed the RMS of the differences between CE318-T and MICROTOPS II is 0.0149, 0.0128, 0.0099 and 0.0090 at 380, 440, 500 and 870. This is in good agreement with the results from land-based comparison by Ichoku et al. (2002), which stated the difference between clean calibrated MICROTOPS II and the AERONET Sun photometer is 0.02 at 380 nm and decreasing down to 0.01 at 870 nm. Detailed comparison results can be found in table 1.

Table 1 Statistics for Comparison Dataset between CE318-T and MICROTOPS II

wavelength (nm)	mean difference (*d*)	RMS of differen ce (*s*)	upper limit of bound (*d+1.96s*)	lower limit of bound *(d-1.96s)*	independ ence test	Chi2 test for normal distributio n	Percentage of outside of bound
380	0.0019	0.0149	0.0311	-0.0274	pass	fail	3.8
440	0.005	0.0128	0.0301	-0.0201	pass	fail	3.8
500	0.0052	0.0099	0.0247	-0.0142	pass	fail	7.59
870	0.0027	0.009	0.0203	-0.0148	pass	fail	2.53

In the comparison, we found the difference of AODs at 4 wavelengths failed the chi2 test for normal distribution, which means there were system errors either in MICROTOPS II or in shipborne CE318-T. Based on the current dataset, we cannot point out which one was responsible for this. However, the RMS difference still showed very good agreement, which is even at the limit of MICROTOPS II measurement error (Ichoku et al., 2002).

Also, why just present AOD (500) and Angstrom? I think a comparison of all available bands would be useful.

AR: The idea for showing AOD comparisons only at 500 nm is because this wavelength (532 nm) was commonly used in lidar community. But triggered by your comment, statistical analysis for the AOD at 5 wavelengths were also added in Sect. 3.1.1 and Figure 4 was reproduced for the comparisons at 4 wavelengths.

In general, all of them are in good agreement.

In any case, I hope that I have not discouraged the authors from continuing with this important paper. I sincerely hope that this can be published in a form that is useful to the community. I think most of my comments can be addressed with more detailed descriptions, with the exception of section 3.2.

AR: The comments are very informative and friendly. We also hope the paper can be informative and valuable to our community.

Detailed comments follow:

Page 1 Line 26: "cannot be used to resolve diurnal cycle of the boundary layer" ->perhaps too strong of a statement considering new geostationary observations.

AR: Yes, we agree. And it's not really reasonable to mention the capability of capturing the boundary layer structure as compared with sunphotometer. Because the latter one cannot capture it, either. We revised this sentence with "Spaceborne aerosol observations are available but most of them work in low earth orbit, which can not be used to resolve regional aerosol conditions as a function of time."

Page 1 Line 30: AERONET-MAN was actually proceeded by a NASA program called SIMBIOS (Sensor Intercalibration and Merger for Biological and Interdisciplinary Oceanic Studies), …

AR: Thanks for pointing out this and we are very glad to know more details and history about MAN and also SIMBIOS. But since we didn't really focus on SIMBOS, we finally decided to only add a brief mention about this in Sect. 2.2.

'The Maritime Aerosol Network (MAN), which was proceeded by SIMBIO (Sensor Intercalibration and Merger for Biological and Interdisciplinary Oceanic Studies) (Fargion et al., 2001; Knobelspiesse et al., 2004), was working as a component of …'

Page 3, line 4: "AOD shift of 0.002" it is not clear which (later) analysis this is referring to

AR: This was concluded by the offset of the linear regression. However, according to Bland-Altman plot, this AOD shift, or the mean difference, at 380, 440, 500 and 870 nm were 0.0019, 0.0050, 0.0052 and 0.0027.

Therefore, we replaced "AOD shift of 0.002" with "mean difference of 0.0019, 0.0050, 0.0052 and 0.0027 at …".

Page 3, lines 8-11: this is where I would have liked more of a description between the differences between the ship-based CE318-T, and the land based version.

AR: This whole section was extended according to the previous comments. Please check the revisions in Sect. 2.1.

Page 3, line 14: What is the wind speed / sea state shut off based on the anemometer? Are there other mechanisms that would shut off the instrument other than clouds and rain?

AR: We set the maximum wind speed as 40 km/h. This threshold was chosen based on our experience of instrument vibration due to strong winds. This threshold worked quite well for the whole period.

Regarding other shutdown mechanisms, we only took the wind and rain into account, which was enough for us to ensure high quality measurements according to the results from these two Polarstern cruises.

Page 3, line 19: I think you can't expect that all readers would know what level 1.5 means, this should be explained.

AR: Thanks for reminding us of this. We added some sentences in Sect 2.1.1 to explain the meaning of different data levels.

"There are three data quality levels for the AOD both from shipborne CE318-T and MICROTOPS II: Level 1.0 with no cloud screening, Level 1.5 with cloud screening and Level 2.0 (Level 1.6 for shipborne CE318-T) for cloud screening and quality assurance (Smirnov et al., 2011). We only use Level 2.0 (Level 1.6 for shipborne CE318-T) for the analysis."

Page 3, line 21: "In the framework of MAN" is vague, are you saying that it is a MAN instrument, or another Microtops that is calibrated, etc. the same way? If the latter, how is this done, specifically?

AR: It's an MAN instrument and was sent and calibrated by NASA Goddard Space Flight Center. So it had the same measurement protocol and data quality as other MAN instrument.

In order to make it clear, we change the sentence of "… performed with a handheld MICROTOPS II in the framework of MAN" as "… performed with a handheld MICROTOPS II from NASA Goddard Space Flight Center, which was a standardized MAN instrument."

Page 5, line 10: I'm assuming the +/- values are standard deviations, but it wouldn't hurt to say it.

AR: Yes, it's the standard deviations. We kept the conventions applied in many lidar data analysis paper. In order to clarify this, we mentioned in Sect 3.2.1 (with red color) that "0.06 ± 0.01 ('±' means standard deviations)"

Page 6, line 19: "free of pollution" Do you mean to say free of fine mode aerosols? I would assume there is a lot of smoke here, but some of it might be natural.

AR: We are sorry about this statement. I just copied and pasted it by mistake in the final editing. We deleted this in the new version.

Page 7, line 6: I must assume that between 0:00 and 7:00 UTC is nighttime, but this is never mentioned. What is the local UTC offset, and sun rise and sun set? Seems like an important part of this analysis. It should also be shown in Figure 6, probably easy to indicate with vertical lines at sunrise/set

AR: The labels and white vertical lines for sunrise and sunset were added in Figure 6.

Page 7, lines 13-14: You conclude that the MBL was contaminated by dust and smoke...but this section set out to demonstrate how well day and night sun photometer observations agree, right? Why isn't that discussed instead? And why are the issues mentioned in the conclusions mentioned?

AR: Our original idea for the case studies is not only including the comparisons but also showing our analysis about aerosol conditions, since we are most interested in the aerosols. But as we came back to read this part again, we found this could be misleading for the readers to extract the messages. Therefore, we removed the aerosol analysis, and put the conclusion about the comparison in the end to highlight the topic.

Thanks for pointing out this.

Page 7, lines 18-30: This analysis, and figure 13 are fine, I guess, but considering that the range of locations span two hemispheres and weeks of time, I think this can't be used to demonstrate that Microtops and Cimel agree. Yes, they both capture the transition from maritime to African smoke/dust plumes and back again, but those are such large features as to not really illustrate the differences between the instruments.

AR: Yes, this figure and the analysis are about the aerosol conditions, not purely about the instrument comparison. Because we thought the latitudinal distribution can give us an overview about the aerosol conditions along the cruise, and tell us that the Atlantic ocean was the playground of dust, smoke and anthropogenic aerosols, not only filled with sea salt.

In the revised manuscript, we moved it to Sect. 3.2.2 to introduce the case studies.

Page 8, conclusions: see my previous comments, these seem unsupported by the previous material.

AR: The unsupported conclusions now have been removed. And it was discussed in Sect 3.1.1.

Page 11, line 8: This isn't really a citation for MAN. At the very least provide the website address. Or cite the Smirnov 2009 paper instead.

AR: Sorry for the wrong citations. We added the link to the MAN data download page.

Page 20, line 9: You mention the color red for pure marine conditions in fig 4, on my version of the figure this is marked in blue.

AR: We have revised the text and used the blue color to represent pure marine conditions in fig 4(now at Figure 6).

References

Fargion, G. S., Barnes, R., and McClain, C.: In Situ Aerosol Optical Thickness Collected by the SIMBIOS Program (1997-2000): Protocols, and and Data QC and Analysis, 2001.

Ichoku, C., Levy, R., Kaufman, Y. J., Remer, L. A., Li, R. R., Martins, V. J., Holben, B. N., Abuhassan, N., Slutsker, I., and Eck, T. F.: Analysis of the performance characteristics of the five-channel Microtops II Sun photometer for measuring aerosol optical thickness and precipitable water vapor, Journal of Geophysical Research: Atmospheres, 107, AAC 5-1-AAC 5-17, https://doi.org/10.1029/2001jd001302, 2002.

Knobelspiesse, K., Tan, Q., Bruegge, C., Cairns, B., Chowdhary, J., van Diedenhoven, B., Diner, D., Ferrare, R., van Harten, G., and Jovanovic, V.: Intercomparison of airborne multi-angle polarimeter observations from the Polarimeter Definition Experiment, Applied optics, 58, 650-669, https://doi.org/10.1364/ao.58.000650, 2019.

Knobelspiesse, K. D., Pietras, C., Fargion, G. S., Wang, M., Frouin, R., Miller, M. A., Subramaniam, A., and Balch, W. M.: Maritime aerosol optical thickness measured by handheld sun photometers, Remote Sensing of Environment, 93, 87-106, https://doi.org/10.1016/j.rse.2004.06.018, 2004.

Smirnov, A., Holben, B. N., Giles, D. M., Slutsker, I., O'Neill, N. T., Eck, T. F., Macke, A., Croot, P., Courcoux, Y., Sakerin, S. M., Smyth, T. J., Zielinski, T., Zibordi, G., Goes, J. I., Harvey, M. J., Quinn, P. K., Nelson, N. B., Radionov, V. F., Duarte, C. M., Losno, R., Sciare, J., Voss, K. J., Kinne, S., Nalli, N. R., Joseph, E., Moorthy, K. K., Covert, D. S., Gulev, S. K., Milinevsky, G., Larouche, P., Belanger, S., Horne, E., Chin, M., Remer, L. A., Kahn, R. A., Reid, J. S., Schulz, M., Heald, C. L., Zhang, J., Lapina, K., Kleidman, R. G., Griesfeller, J., Gaitley, B. J., Tan, Q., and Diehl, T. L.: Maritime aerosol network as a component of AERONET - first results and comparison with global aerosol models and satellite retrievals, Atmospheric Measurement Techniques, 4, 583-597, https://doi.org/10.5194/amt-4-583-2011, 2011.

WMO, W.: GAW Experts Workshop on a Global Surface Based Network for Long Term Observations of Column Aerosol Optical Properties, edited by U. Baltensperger, L. Barrie, C. Wehrli, GAW Report,

Response to Anonymous Referee #2

General comments:

"My main critique of the manuscript is that the authors do not do enough to show the significance of their contribution. …"

AR: We agree. We firstly explained the reason for this in the beginning of this reply letter. We want to emphasize that our idea for this paper was to validate the shipborne CE318-T and deliver two messages to the readers. First, the current status of this instrument was applicable to capture the aerosol conditions unattended over the vast ocean. And the dataset can be incorporated into lidar data analysis, which is a great advantage for extracting vertical information about marine aerosols.

According to our knowledge, such research was never published before with using the CE318-T on-board a ship and it was also the first time to apply the collocated MICROTOPS II and advanced multiwavelength Raman lidar to validate the daytime and nighttime AOD measurements, respectively.

Besides, we want to add one more point that this instrument will join the unprecedented MOSAiC campaign, which could be important for our better understanding of global climate change. Therefore, our analysis will also lay down the foundation for the our future data analysis.

Specific comments:

"The literature review of the AOD measurements of marine aerosols and their significance is insufficient – the authors should try to provide a better picture of what has been already done and how their work contributes to the pool of knowledge."

AR: We add two more paragraphs to better explain the status and importance regarding marine aerosols measurements in the introduction (in red).

"Ocean covers more than 70 % of our planet earth, and works as one of the largest natural aerosol sources. Marine aerosols, generated from the oceanic white cap and bubble bursting, impose significant contributions to the global direct radiative forcing (Satheesh and Moorthy, 2005). Meanwhile, the transported aerosols from the continent, which complicates the aerosols conditions over the ocean, also plays an important role. The corresponding measurements by passive remote sensing can be done by spaceborne, airborne or shipborne platforms. Spaceborne measurements can provide a global picture of the aerosol conditions over a long-term. But for the data retrievals in the current stage, they still require assumptions about the terrain (Hsu et al., 2013; Sayer et al., 2018). Airborne measurements have a large coverage (Karol et al., 2013), but the cost for each flight is high and the airplane itself is sensitive to the weather conditions, which makes it less available for long-term observations. Shipborne measurements has been done over a long time (Smirnov et al., 2002; Knobelspiesse et al., 2004). Although it's also challenging compared with land-based

measurements due to the mobility of the platform and severe weather conditions, huge progress of sun photometer technologies (Karol et al., 2013; Barreto et al., 2016; Livingston et al., 2003) has been made over more than 20 years since the beginning of the NASA Sensor Inter-comparison and Merger for Biological and Interdisciplinary Oceanic Studies (SIMBIOS)(Fargion et al., 1999), which is dedicated for intercalibration and validation for ocean color satellites."

Besides, the answer to the question "How their work contributes to the pool of knowledge" can also be found in line 22-30, page 2.

"Since comparing CE318T and PollyXT AOD is a significant part of the analysis, it should be clearly shown how AOD estimated from sunphotometry relates to PollyXT measurements through extinction (I could not find a single formula in the entire paper!) Also, I found practically no discussion of error analysis of the derived quantities."

AR: A short answer to this comment. Raman method (Ansmann et al., 1990) has been widely used to obtain aerosol extinction coefficient with Raman Lidar. There are many literatures, documents and presentations (Ansmann et al., 1992; Mattis et al., 2016; Groß et al., 2011b; Whiteman, 1999; Baars et al., 2016) to discuss how it works and how the uncertainty was over more than 20 years. We think doing it again will not bring any new knowledge about this topic and on the contrary, it will make the whole paper cumbersome. Therefore, we decide to present error analysis only in the reply letter. Regarding the revision in the manuscript, we summarized the total relative error for AOD in Sect. 2.3, and also add the error bar to Figure 8

Explanation about error analysis of aerosol extinction coefficient with Raman method.

Extinction coefficient can be retrieved from Raman lidar measurements (Eq. 1) (Sect. 4.1(Groß et al., 2011b)).

$$\alpha_p(z,\lambda_0) = \left(1 + f_p\right)^{-1}\left\{\frac{1}{\alpha_m(z,\lambda_0)}\frac{d\alpha_m(z,\lambda_0)}{dz} - \frac{1}{X(z,\lambda_R)}\frac{dX(z,\lambda_R)}{dz} - (1 + f_m)\alpha_m(z,\lambda_0)\right\} (1)$$

In which, λ_0 and λ_R are the wavelengths of emitting laser pulse and Raman scattering, respectively. f_p and f_m are used to describe the wavelength dependence of extinction coefficient from aerosols and air molecules, which are defined as below

$$f_p = \left(\frac{\lambda_0}{\lambda_R}\right)^{\text{Å}} (2)$$

$$f_m = \left(\frac{\lambda_0}{\lambda_R}\right)^{4.085} (3)$$

α_m is the extinction coefficient of air molecules, which can be calculated with high accuracy with the temperature and pressure profile from collocated radiosonde or reanalysis data. $X(z,\lambda_R)$ is the range corrected signal, which is defined as below:

$$X(z,\lambda_R) = CO(z)P(z,\lambda_R)z^2 (4)$$

C is the lidar constant which relates to the system efficiency. $O(z)$ is the overlap function, which states the fraction of the overlap area between laser beam and the field of view of the telescope. The overlap function can be treated as a unity above certain altitude and this altitude is related with the divergence of the laser beam and field of view (FOV) of the telescope. For our lidar system, these altitude are 120 and 800 m for near-range (NR) and far-range (FR) channels, respectively. And $P(z, \lambda_R)$ is the measured signal from Raman channel.

The error of the extinction coefficient can be divided into 2 parts: systematic (**syst**) and statistical (**ran**) error. (Sect. 4.1(Groß et al., 2011b))

$$\Delta\alpha_p^{syst}(z, \lambda_0) = \left|\frac{\partial\alpha_p(z, \lambda_R)}{\partial f_p(z)} \cdot \Delta f_p(z)\right| + \left|\frac{\partial\alpha_p(z, \lambda_R)}{\partial\alpha_m(z, \lambda_R)} \cdot \Delta\alpha_m(z, \lambda_R)\right| (2)$$

$$\Delta\alpha_p^{ran}(z, \lambda_0) = \sqrt{\left(\frac{\partial\alpha_p(z, \lambda_R)}{\partial X(z, \lambda_R)} \cdot \Delta X(z, \lambda)\right)^2 + \left(\frac{\partial\alpha_p(z, \lambda_R)}{\partial C_X(z)} \cdot \Delta C_X^{ran}(z)\right)^2} (3)$$

The systematic error comes from the deviations of the applied Å and molecular extinction coefficient to the truth. For the first part, we took Å from the MICROTOPS II into Raman retrieval, which is 0.6 for the smoke case at November 26 2018. And we finally use the standard deviation (std) of 0.1 to represent the error of Å, which yields a relative error of ~ 0.6 % for extinction coefficient. For the latter part of the systematic error, which came from the variations of molecular density over space and time. According to Mattis et al. (2004), the relative error introduced by the uncertainties with using the temperature and pressure profiles from radiosonde is of the order of 1%-5%. For Raman retrieval, we use the reanalysis data from GDAS1, which has very high accuracy about temperature and pressure compared with radiosonde (Dai et al., 2018). Therefore, the contribution of systematic error should be also at the order of 1%-5%.

The statistical error was contributed by the signal noise (the first term in Eq. 3) and the error of the least-square fit (the second term in Eq. 3, in which, $C_X = \frac{dX(z, \lambda_R)}{dz}$). These two terms can be calculated individually and is related with signal-noise-ratio (SNR). In order to achieve high SNR, we accumulate the nighttime Raman signal within 1 hour and using the smoothing window with 21 bins and 51 bins for NR and FR channels, respectively, to ensure the relative uncertainty was less than 10 % up to 6 km.

We then use the integration of aerosol extinction coefficient to calculate the AOD, with the formula below

$$\tau(\lambda_0, z_0) = \int_0^{z_0} \alpha_p(\lambda_0, z')dz', \ z_0 = 6 \text{ km}$$

where $\tau(\lambda_0, z_0)$ is the aerosol optical depth from ground to z_0 at the wavelength λ_0. Because the extinction coefficient was influenced by the overlap function at near-ground, we then combined the extinction coefficients with the near-range and far-range Raman signal to cover from 120 m to 6 km. And using a constant value at 120 m to represent the aerosol extinction coefficient from ground to 120 m, which caused an error of AOD around 0.005. Besides, we also checked the signal compared with Rayleigh signal to exclude aerosol layers above 6 km for the case on 26 November 2018.

Therefore, in total, the error of AOD from lidar measurements was **11%-15%**, which is 0.04-0.06 at 532 nm, with taking into account of the mean AOD of 0.4.

"There should be a more detailed discussion of the cloud screening techniques and their influence on the results."

AR: We need to point out that the data analysis for shipborne CE318-T is nearly the same with AERONET data processing and the only difference is that we need to take care of the geolocation, which was set fixed for AERONET data processing. For the cloud-screening techniques, we follow the triplet stability criterion of AERONET (Smirnov et al., 2000), with $(\tau_{max} - \tau_{min}) < \max\{\tau_{min} * 0.03, 0.02\}$. This is very similar to the cloud-screen techniques applied for MAN data processing (Smirnov et al., 2009), which is $(\tau_{max} - \tau_{min}) < \max\{\tau_{min} * 0.05, 0.02\}$. Although there was manual inspection to further screen out the effects from cloud contamination for MAN data processing, but within our comparisons (see Figure 4), we didn't see any outliers, which states the minor difference of the criteria didn't contribute to strong influences on the comparisons.

"The manuscript should be proofread for multiple English errors scattered throughout the document – I'm only pointing out some of them. Phrases like "slightly enhanced", "quite low" or even simply "large" or "small" need to be quantified. The word "probably" is used too many times and by itself is not adequate when discussing scientific findings."

AR: Thanks for pointing out this. The awkward English phrases and expressions have been fixed and we went over the whole manuscript and revise other places as well (in red).

"P1L27: "ARE very challenging""

AR: done

"P2L1: "transport" rather than "transportation"?"

AR: done and fixed other parts with the same wrong words at the same time.

"P2L10: why only almucantar measurements are discussed? Is your Cimel not capable of Principal Plane measurements?"

AR: Regarding the Principal Plane measurements, in theory, it can be done. But it's not our objective for this instrument at the moment, that's why we didn't mention that.

"P2L29: "The instruments are scheduled" is awkward phrasing"

AR: It has been revised to "The instruments are dedicated for investigating aerosol cloud and …"

"P3L6: I feel that calling it a "prototype CE318-T" is misleading since no changes were made to the instrument itself but rather to the platform on which it operates. It would be interesting to see a picture or an engineering diagram of this modification"

AR: We agree with your argument for the misleading calling, because main new features of this shipborne CE318-T were about the ancillary devices and on the software level. In general, the upgrades were done in three aspects: new compass for orientation measurements, air pumping system for isolating the sea spray and new tracking software to deal with the variable geolocation and orientation. We don't have the engineering diagram of the air pumping system at this moment, because this is an experimental instrument. The pictures about the base and the diagram of the air pumping system was attached below to throw some light on this topic.
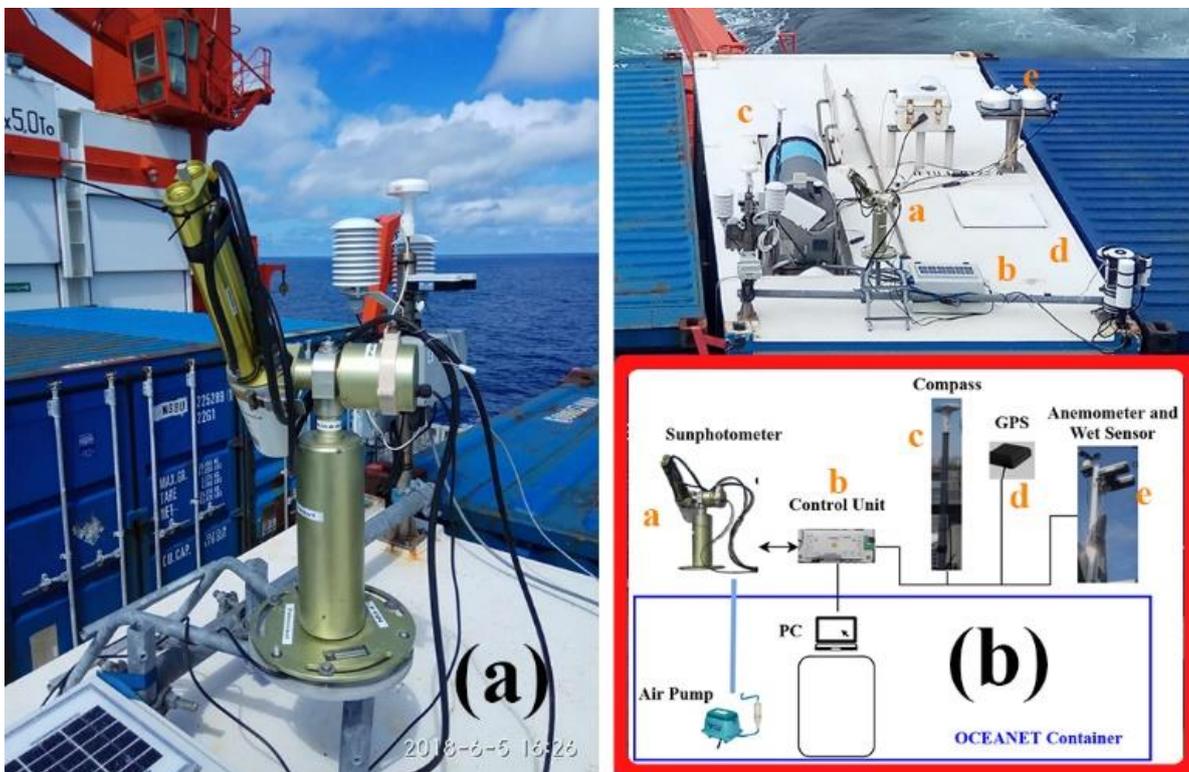
Figure 1 picture of the optical head and tracking base over the OCEANET container and schematic.
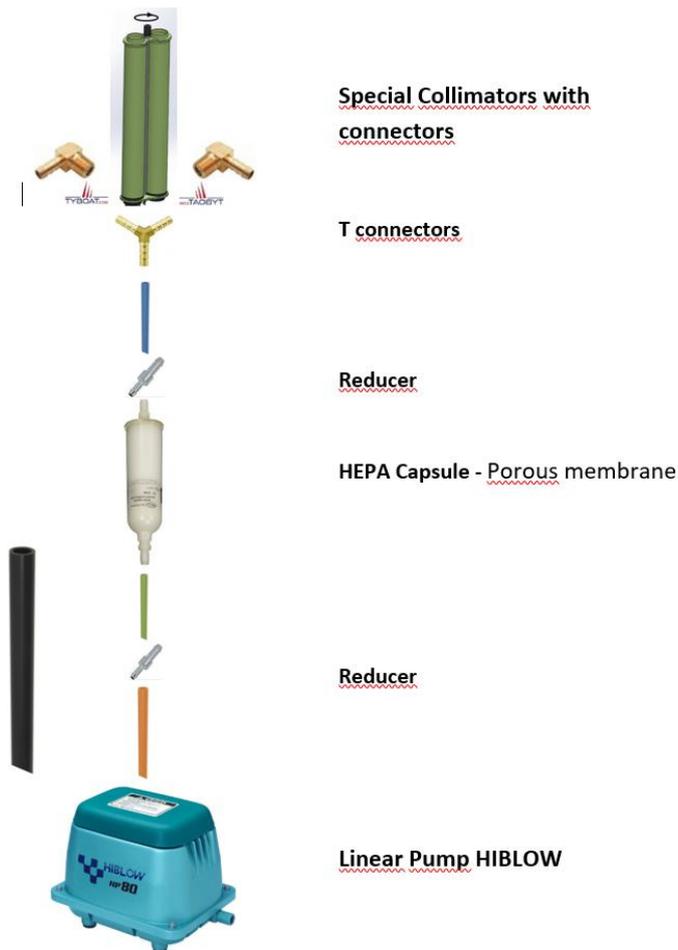
Figure 2 Schematic of the air pumping system

"**P3L25: This section should be reworked. The section discusses backscatter and extinction coefficients (presumably derived directly from Raman technique) next to the lidar ratio and (further in the article) Fernald methodology. It should be stated which quantities are measured directly and which are estimated. "Far-range" and "near-range" should be quantified. "Total and cross" should be defined.**"

AR: Yes, we agree.

What the lidar can directly measures is the backscatter signal from air molecules and particles.

The quantities of extinction and backscatter coefficients, lidar ratio, particle depolarization ratio and etc., are all retrieved either with Raman method or Fernald method. Raman method only needs the assumption about wavelength dependence of extinction coefficient, for getting all those quantities. This assumption contributes to uncertainties of 10.5% for extinction coefficient at the extreme conditions (Veselovskii et al., 2015). For Fernald method, it needs the

13

assumption of lidar ratio, which can be erroneous, but it can be constrained with using the collocated sunphotometer measurements (Heese et al., 2010).

Now the Sect. 2.3 was re-worked. The changes triggered by your comments were marked with red color.

"P4L7. Not sure what is being meant here by "These intensive parameters are sensitive to particle size, shape and chemistry properties". Which parameters? Angstrom exponent? Particle size and shape are themselves intensive parameters (i.e. are per particle rather than bulk properties)."

AR: Sorry for the misleading expression. The "intensive parameters", namely Ångström exponent and particle depolarization ratio (Amiridis et al., 2015), should be replaced with "intensive properties", which is related to the particle size and shape.

"P5L4. Why do the authors present the "attenuated backscatter coefficient" rather than
the extinction coefficient more relevant to AOD comparisons?"

AR: This is because we want to show the temporal-spatial variations of the marine aerosols. Extinction coefficient with Raman method cannot be retrieved in such high resolution with our instrument, due to the weak Raman signal at daytime. The attenuated backscatter itself is also a good indicator if only marine aerosol is present, since the lidar ratio is well characterized for pure marine aerosols, at 25 sr from other measurements (Bohlmann et al., 2018; Haarig et al., 2017).

"P5L14. The Fernald/Klett method and the choice of the lidar ratio should first be discussed in the methodology section."

AR: We agree with you. However, Fernald/Klett method has been applied for more than 40 years, there are plenty of articles going into this topic. It's not our objective to show the details about how errors with Fernald/Klett method was calculated, although we have done that for our data analysis and also included the error bars in the averaged profiles in Figure 14. We thought providing some numbers about the error should be sufficient for the general readers who are not lidar expert. Therefore, we added some sentences in Sect 2.3 and referred to the work of (Hughes et al., 1985; Rocadenbosch and Comeron, 1999) to provide the door to know more. See the new Sect. 2.3.

"P5L18. The last two sentences of the section should use references"
AR: It has been done.

"P6L4 Which "reference values"? What does it mean "tuned to achieve the best agreement of AOD"? How does it affect your results/comparisons?"

AR: The "reference values" means the aerosol backscatter coefficient at the reference height. Normally, if the signal is strong enough to arrive top of troposphere or even stratosphere, we will set the values to 0, because it's nearly aerosol-free at this high altitude. But at daytime and under strong attenuation by dense aerosol plumes, it's hardly to find the aerosol-free height with good SNR.

If the reference values were larger than the true values, the whole profile would be larger and vice versa(Rocadenbosch and Comeron, 1999; Matsumoto and Takeuchi, 1994). Therefore, one has to use other measurements to constrain the reference values. One way to do this is to use the AOD from collocated sunphotometer measurements (Heese et al., 2010). The lidar ratio was taken from nighttime measurements with Raman method, which was valid if the aerosol layer was stable and continuous. In this way, we can retrieve the optical properties of the severe dust storm. The influences of this method was dependent on the lidar ratio and the spatial difference of the detection area between lidar and sunphotometer. For the Saharan dust case in Sect. 3.2, the zenith angle of the sunphotometer is 56° and the optical depth as you can see in Figure 13 is stable over the measurement window of 1 hour. Meanwhile, the retrieved optical properties of dust layer agreed with the results from other literatures (Groß et al., 2011a; Tesche et al., 2009; Rittmeister et al., 2017).

References

Amiridis, V., Marinou, E., Tsekeri, A., Wandinger, U., Schwarz, A., Giannakaki, E., Mamouri, R.-E., Kokkalis, P., Binietoglou, I., and Solomos, S.: LIVAS: a 3-D multi-wavelength aerosol/cloud database based on CALIPSO and EARLINET, 2015.

Ansmann, A., Riebesell, M., and Weitkamp, C.: Measurement of atmospheric aerosol extinction profiles with a Raman lidar, Opt. Lett., 15, 746-748, https://doi.org/10.1364/OL.15.000746, 1990.

Ansmann, A., Riebesell, M., Wandinger, U., Weitkamp, C., Voss, E., Lahmann, W., and Michaelis, W.: Combined Raman Elastic-Backscatter Lidar for Vertical Profiling of Moisture, Aerosol Extinction, Backscatter, and Lidar Ratio, Appl Phys B-Photo, 55, 18-28, https://doi.org/10.1007/Bf00348608, 1992.

Baars, H., Kanitz, T., Engelmann, R., Althausen, D., Heese, B., Komppula, M., Preissler, J., Tesche, M., Ansmann, A., Wandinger, U., Lim, J. H., Ahn, J. Y., Stachlewska, I. S., Amiridis, V., Marinou, E., Seifert, P., Hofer, J., Skupin, A., Schneider, F., Bohlmann, S., Foth, A., Bley, S., Pfuller, A., Giannakaki, E., Lihavainen, H., Viisanen, Y., Hooda, R. K., Pereira, S. N., Bortoli, D., Wagner, F., Mattis, I., Janicka, L., Markowicz, K. M., Achtert, P., Artaxo, P., Pauliquevis, T., Souza, R. A. F., Sharma, V. P., van Zyl, P. G., Beukes, J. P., Sun, J. Y., Rohwer, E. G., Deng, R. R., Mamouri, R. E., and Zamorano, F.: An overview of the first decade of Polly(NET): an emerging network of automated Raman-polarization lidars for continuous aerosol profiling, Atmospheric Chemistry and Physics, 16, 5111-5137, https://doi.org/10.5194/acp-16-5111-2016, 2016.

Barreto, A., Cuevas, E., Granados-Munoz, M. J., Alados-Arboledas, L., Romero, P. M., Grobner, J., Kouremeti, N., Almansa, A. F., Stone, T., Toledano, C., Roman, R., Sorokin, M., Holben, B., Canini, M., and Yela, M.: The new sun-sky-lunar Cimel CE318-

T multiband photometer - a comprehensive performance evaluation, Atmospheric Measurement Techniques, 9, 631-654, https://doi.org/10.5194/amt-9-631-2016, 2016.

Bohlmann, S., Baars, H., Radenz, M., Engelmann, R., and Macke, A.: Ship-borne aerosol profiling with lidar over the Atlantic Ocean: from pure marine conditions to complex dust-smoke mixtures, Atmospheric Chemistry and Physics, 18, 9661-9679, https://doi.org/10.5194/acp-18-9661-2018, 2018.

Dai, G., Althausen, D., Hofer, J., Engelmann, R., Seifert, P., Bühl, J., Mamouri, R.-E., Wu, S., and Ansmann, A.: Calibration of Raman lidar water vapor profiles by means of AERONET photometer observations and GDAS meteorological data, Atmospheric Measurement Techniques, 11, 2735-2748, 2018.

Fargion, G. S., McClain, C. R., Fukushima, H., Nicolas, J. M., and Barnes, R. A.: Ocean color instrument intercomparisons and cross-calibrations by the SIMBIOS Project, Sensors, Systems, and Next-Generation Satellites III, 1999, 397-403,

Groß, S., Tesche, M., Freudenthaler, V., Toledano, C., Wiegner, M., Ansmann, A., Althausen, D., and Seefeldner, M.: Characterization of Saharan dust, marine aerosols and mixtures of biomass-burning aerosols and dust by means of multi-wavelength depolarization and Raman lidar measurements during SAMUM 2, Tellus B: Chemical and Physical Meteorology, 63, 706-724, https://doi.org/10.3402/tellusb.v63i4.16369, 2011a.

Groß, S., Wiegner, M., Freudenthaler, V., and Toledano, C.: Lidar ratio of Saharan dust over Cape Verde Islands: Assessment and error calculation, Journal of Geophysical Research: Atmospheres, 116, https://doi.org/10.1029/2010JD015435, 2011b.

Haarig, M., Ansmann, A., Gasteiger, J., Kandler, K., Althausen, D., Baars, H., Radenz, M., and Farrell, D. A.: Dry versus wet marine particle optical properties: RH dependence of depolarization ratio, backscatter, and extinction from multiwavelength lidar measurements during SALTRACE, Atmospheric Chemistry and Physics, 17, 14199, https://doi.org/10.5194/acp-2017-545, 2017.

Heese, B., Flentje, H., Althausen, D., Ansmann, A., and Frey, S.: Ceilometer lidar comparison: backscatter coefficient retrieval and signal-to-noise ratio determination, Atmospheric Measurement Techniques, 3, 1763-1770, 2010.

Hsu, N., Jeong, M. J., Bettenhausen, C., Sayer, A., Hansell, R., Seftor, C., Huang, J., and Tsay, S. C.: Enhanced Deep Blue aerosol retrieval algorithm: The second generation, Journal of Geophysical Research: Atmospheres, 118, 9296-9315, 2013.

Hughes, H. G., Ferguson, J. A., and Stephens, D. H.: Sensitivity of a lidar inversion algorithm to parameters relating atmospheric backscatter and extinction, Applied optics, 24, 1609-1613, https://doi.org/10.1364/ao.24.001609, 1985.

Karol, Y., Tanré, D., Goloub, P., Vervaerde, C., Balois, J., Blarel, L., Podvin, T., Mortier, A., and Chaikovsky, A.: Airborne sun photometer PLASMA: concept, measurements, comparison of aerosol extinction vertical profile with lidar, Atmospheric Measurement Techniques, 6, 2383-2389, https://doi.org/10.5194/amt-6-2383-2013, 2013.

Knobelspiesse, K. D., Pietras, C., Fargion, G. S., Wang, M., Frouin, R., Miller, M. A., Subramaniam, A., and Balch, W. M.: Maritime aerosol optical thickness measured by handheld sun photometers, Remote Sensing of Environment, 93, 87-106, https://doi.org/10.1016/j.rse.2004.06.018, 2004.

Livingston, J. M., Russell, P. B., Reid, J. S., Redemann, J., Schmid, B., Allen, D. A., Torres, O., Levy, R. C., Remer, L. A., and Holben, B. N.: Airborne Sun photometer measurements of aerosol optical depth and columnar water vapor during the Puerto Rico

Dust Experiment and comparison with land, aircraft, and satellite measurements, Journal of Geophysical Research: Atmospheres, 108, 2003.

Matsumoto, M., and Takeuchi, N.: Effects of misestimated far-end boundary values on two common lidar inversion solutions, Applied Optics, 33, 6451-6456, https://doi.org/10.1364/AO.33.006451, 1994.

Mattis, I., Ansmann, A., Müller, D., Wandinger, U., and Althausen, D.: Multiyear aerosol observations with dual-wavelength Raman lidar in the framework of EARLINET, Journal of Geophysical Research: Atmospheres, 109, https://doi.org/10.1029/2004jd004600, 2004.

Mattis, I., D'Amico, G., Baars, H., Amodeo, A., Madonna, F., and Iarlori, M.: EARLINET Single Calculus Chain–technical–Part 2: Calculation of optical products, Atmospheric Measurement Techniques, 9, 3009-3029, 2016.

Rittmeister, F., Ansmann, A., Engelmann, R., Skupin, A., Baars, H., Kanitz, T., and Kinne, S.: Profiling of Saharan dust from the Caribbean to western Africa-Part 1: Layering structures and optical properties from shipborne polarization/Raman lidar observations, Atmospheric Chemistry and Physics, 17, 12963-12983, https://doi.org/10.5194/acp-17-12963-2017, 2017.

Rocadenbosch, F., and Comeron, A.: Error analysis for the lidar backward inversion algorithm, Applied optics, 38, 4461-4474, 1999.

Satheesh, S., and Moorthy, K. K.: Radiative effects of natural aerosols: A review, Atmospheric Environment, 39, 2089-2110, 2005.

Sayer, A., Hsu, N., Lee, J., Bettenhausen, C., Kim, W., and Smirnov, A.: Satellite Ocean Aerosol Retrieval (SOAR) Algorithm Extension to S-NPP VIIRS as Part of the "Deep Blue" Aerosol Project, Journal of Geophysical Research: Atmospheres, 123, 380-400, 2018.

Smirnov, A., Holben, B., Eck, T., Dubovik, O., and Slutsker, I.: Cloud-screening and quality control algorithms for the AERONET database, Remote sensing of environment, 73, 337-349, 2000.

Smirnov, A., Holben, B. N., Kaufman, Y. J., Dubovik, O., Eck, T. F., Slutsker, I., Pietras, C., and Halthore, R. N.: Optical properties of atmospheric aerosol in maritime environments, Journal of the Atmospheric Sciences, 59, 501-523, 2002.

Smirnov, A., Holben, B. N., Slutsker, I., Giles, D. M., McClain, C. R., Eck, T. F., Sakerin, S. M., Macke, A., Croot, P., Zibordi, G., Quinn, P. K., Sciare, J., Kinne, S., Harvey, M., Smyth, T. J., Piketh, S., Zielinski, T., Proshutinsky, A., Goes, J. I., Nelson, N. B., Larouche, P., Radionov, V. F., Goloub, P., Moorthy, K. K., Matarrese, R., Robertson, E. J., and Jourdin, F.: Maritime Aerosol Network as a component of Aerosol Robotic Network, J Geophys Res-Atmos, 114, https://doi.org/10.1029/2008jd011257, 2009.

Tesche, M., Ansmann, A., Muller, D., Althausen, D., Mattis, I., Heese, B., Freudenthaler, V., Wiegner, M., Esselborn, M., Pisani, G., and Knippertz, P.: Vertical profiling of Saharan dust with Raman lidars and airborne HSRL in southern Morocco during SAMUM, Tellus Series B-Chemical and Physical Meteorology, 61, 144-164, https://doi.org/10.1111/j.1600-0889.2008.00390.x, 2009.

Veselovskii, I., Whiteman, D., Korenskiy, M., Suvorina, A., and Pérez-Ramírez, D.: Use of rotational Raman measurements in multiwavelength aerosol lidar for evaluation of particle backscattering and extinction, Atmospheric Measurement Techniques, 8, 4111-4122, 2015.

Whiteman, D. N.: Application of statistical methods to the determination of slope in lidar data, Applied optics, 38, 3360-3369, 1999.

Aerosol measurements with shipborne sun-sky-lunar photometer and collocated multiwavelength Raman polarization lidar over the Atlantic Ocean

Zhenping Yin[1,2,3], Albert Ansmann[1], Holger Baars[1], Martin Radenz[1], Cristofer Jimenez[1], Ronny Engelmann[1], Patric Seifert[1], Alina Herzog[1], Kevin Ohneiser[1], Karsten Hanbuch[1], Luc Blarel[4], Philippe Goloub[4], Gaël Dubois[4], Stephane Victori[5], Fabrice Maupin[5]

[1]Leibniz Institute for Tropospheric Research, Permoserstraße 15, 04318 Leipzig, Germany
[2]School of Electronic Information, Wuhan University, Wuhan, China
[3]Key Laboratory of Geospace Environment and Geodesy, Ministry of Education, Wuhan, China
[4]Laboratoire d'Optique Amosphérique, Université des Sciences et Technologies de Lille, 59655 Villeneuve d'Ascq, France
[5]Cimel advanced monitoring, Paris, France

Correspondence to: Zhenping Yin (zhenping@tropos.de)

Abstract. A shipborne sun-sky-lunar photometer was tested in two trans-Atlantic cruises aboard the German research vessel *Polarstern* from 54°N to 54°S. A full diurnal cycle of mixed dust-smoke episode measured with shipborne CE318-T is presented for the first time. Latitudinal distribution of AOD from the shipborne CE318-T, Raman lidar and MICROTOPS II shows the same trend with high values ~~at 0 ~ 20°N dust transported belt~~ in the dust belt from 0 ~ 20°N and low values at Southern Hemisphere. Coefficient of determination for the linear regression between MICROTOPS II and shipborne sun-sky-lunar photometer was 0.988, 0.987, ~~0.993~~ 0.994 and 0.994 for AOD at 380, 440, 500 and 870 nm and 0.896 for Ångström exponent at 440-870 nm. Meanwhile, the AOD root-mean-squared differences at 380, 440, 500 and 870 nm are 0.015, 0.013, 0.010 and 0.009.

1 Introduction

Aerosols can influence the Earth radiation budget, e.g., by absorption and scattering of solar radiation, and modulate cloud formation and cloud microphysical properties by serving as cloud condensation nuclei (CCN) or ice nucleating particles (INP). Although great progress has been made ~~about~~ in aerosol observations technologies and climate modeling in recent years, the uncertainty of aerosol radiative forcing in global climate models is still very large due to our poor understanding of aerosol global distribution and aerosol-cloud interactions (Stocker, 2014).

Most of the current aerosol observations are land-based. Spaceborne aerosol observations are available but most of them work in low earth orbit, which can not be used to resolve regional aerosol conditions as a function of time. ~~Although spaceborne aerosol observations are available, they cannot be used to resolve regional aerosol conditions as a function of time, e.g. to resolve the diurnal cycle of the boundary layer.~~

18

~~Observations over the ocean is very challenging compared with land-based measurements due to the mobility of the platform and severe weather conditions.~~ However, the ocean, which covers more than 70 % of our planet earth and works as one of the largest natural aerosol sources, can hardly monitored by land-based instruments. In addition, marine aerosols which are generated from the oceanic white cap and bubble bursting, impose significant contributions to the global direct

5 radiative forcing (Satheesh and Moorthy, 2005). Meanwhile, the transported aerosols from the continent play an important role over the ocean as well, making the aerosol conditions even more complicated. The corresponding measurements for those tiny particles with passive remote sensing intruments can be performed on spaceborne, airborne or shipborne platforms. Spaceborne measurements can provide a global picture of the aerosol conditions over a long-term basis. But the data retrievals require assumptions about the terrain (Hsu et al., 2013; Sayer et al., 2018), which could bring in non-

10 negligible errors. Airborne measurements have a large coverage (Karol et al., 2013), but the cost for each flight is high and the aircraft is sensitive to the weather conditions, which makes it less available for long-term observations. Shipborne measurements has been performed over a long period of time (Smirnov et al., 2002; Knobelspiesse et al., 2004). Although it's also challenging compared with land-based measurements due to the mobility of the platform and severe weather conditions, huge progress about sun photometer technologies (Karol et al., 2013; Barreto et al., 2016; Livingston et al.,

15 2003) has been made over more than 20 years since the start of the NASA Sensor Inter-comparison and Merger for Biological and Interdisciplinary Oceanic Studies (SIMBIOS) (Fargion et al., 1999), which was dedicated to intercalibration and validation for ocean color satellites. The Maritime Aerosol Network (MAN), as a component of the AErosol RObotic NETwork (AERONET), is the largest long-term aerosol observation network over the ocean (Smirnov et al., 2009). It has provided unique dataset about aerosol optical depth (AOD) and precipitable water vapor (PWV) over the ocean even from

20 Arctic to Antarctica. These data ~~is used~~ was taken used in the research about dust ~~transportation~~ transport ~~research~~, satellite retrieval validation and atmospheric correction (Smirnov et al., 2011).

MICROTOPS II is the standard device of MAN. However, it is not dedicated ~~for~~ to automatic maritime network observations. An operator needs to point the photometer to the Sun for a while to ensure stable measurements, which makes it less available for continuous measurements. Moreover, it cannot provide aerosol microphysical properties, including size

25 distribution, scattering phase function and single scattering albedo because of missing sky radiance measurements (Smirnov et al., 2009; Smirnov et al., 2011). Therefore, ~~a prototype of~~ a shipborne photometer based on the ~~most~~ advanced sun-sky-lunar photometer technology (CE318-T)~~, which is aimed at maritime aerosol measurements~~, was developed to cover this gap by the Laboratoire d'Optique Atmosphérique (LOA), Lille, France. This new device has all the capabilities of a land-based CE318-T (Barreto et al., 2016), like AOD measurement from 340 to 1640 nm, PWV measurement,

30 nighttime AOD measurement and almucantar scanning measurement required for the retrieval of aerosol microphysical properties. ~~This new instrument can also be installed on a car and conducts the measurement automatically and~~

continuously. Therefore, it's also easy to be incorporated into AERONET. In addtion, this instrument will be moved to the Arctic on-board RV *Polarstern* with joining the unprecedented Arctic research project MOSAiC (https://www.mosaic-expedition.org/). The dataset regarding the Arctic seasonal aerosol conditions will be definitely helpful to quantify our human effects on global climate change. But before that, we need to address how the shipborne CE318-T setup behaves,

5   how much influence of the sea spray could bring and how about the uncertainty of the AOD measurements under oceanic conditions.

In order to answer these questions, this ~~prototype~~ instrument was tested in the framework of the OCEANET project (Macke et al., 2010) during the past two RV *Polarstern* cruises, PS113 and PS116. PS113 started at Punta Arenas, Chile on 7 May 2018 and ended at Bremerhaven, Germany on 11 June 2018. In the case of PS116, RV *Polarstern* departed from

10   Bremerhaven on 11 November 2018 and arrived at Cape Town on 11 December 2018 (see Fig. Figure for the ship tracks). Equipped with sophisticated ground-based instruments, including a portable and automated Raman and polarization lidar system Polly[XT] (Engelmann et al., 2016; Althausen et al., 2009), microwave radiometer, meteorological station, shadowband radiometer, full-sky imager and MICROTOPS II, it provided a unique opportunity to evaluate the capabilities of the photometer prototype and also provided useful feedback for its future developments.

15   This paper is organised as follows: In Sect. 2, we give a description of the shipborne CE318-T and other applied instruments and data in this paper. ~~Then in Sect. 3.1, we present two detailed case studies to evaluate the performance of the shipborne CE318-T under pure marine conditions and lofted Saharan dust layers.~~ Then in Sect. 3.1, we evaluated the daytime results from the shipborne CE318-T through comparisons with MICROTOPS II and we presented the diurnal measurements of the shipborne CE318-T to validate the nighttime AOD with collocated Raman lidar measurements. In Sect. 3.2, we present

20   two detailed case studies to evaluate the performance of the shipborne CE318-T under pure marine conditions and lofted Saharan dust layers. Besides, we've shown the potential to combine the shipborne CE318-T measurements into lidar data analysis for dust case. ~~Furthermore, we also present full diurnal cycle measurements to investigate the nighttime behaviour of the shipborne CE318-T by comparing the AOD values with the respective ones from Polly[XT] observations. In Sect. 3.2, we show the comparisons between shipborne CE318-T and MICROTOPS II based on the data collected from the two RV~~

25   *Polarstern* cruises. ~~Then, we discuss the latitudinal distribution of AOD and Ångström exponent at 440-870 nm obtained during the two cruises.~~ Finally, in Sect. 4, summarizing and concluding remarks are given.

2 Instrumentation

The instruments of the OCEANET project are scheduled for investigating aerosol cloud and radiation interactions over the remote Atlantic Ocean and contrasting northern with southern hemispheric aerosol and cloud conditions.The OCEANET

project started in the fall of 2009 (Kanitz, 2012). Nearly all the instruments were mounted on the roof of the OCEANET container except the indoor Polly^{XT} lidar. The container was located on the helicopter deck, which is behind the bridge, for these two cruises (see Fig. 2). The MICROTOPS II measurements were conducted on the bridge (see Fig. 2). It should be noted that the 'anthropogenic' smoke from the ~~chimney~~ funnel could contaminate the shipborne CE318-T measurements.

5   However, this was a compromise between avoiding strong head winds, sea spray and smoke. Nevertheless, we only found an AOD shift of 0.002 at 500 nm between shipborne CE318-T and MICROTOPS II, which shows the influence of the smoke was negligible.

2.1 Shipborne CE318-T

The ~~prototype of the~~ shipborne CE318-T is developed to enable AOD measurement over the mobile platform and expand
10   the AERONET coverage to the vast ocean area (Goloub et al., 2017). In principle, the instrument is very similar to the traditional CE318-T (Barreto et al., 2016) and has nearly the same steps for installation ~~procedures~~. The apparatus consists of the optical head, rotational base, control unit, air pumping component, weather stop component, compass and GPS modules (see Fig. 3). The optical head was the same like the other land-based CE318-T. The GPS receiver and compass module (SIMRAD HS60) were fixed on the platform together with the photometer robot to assure the same motions. In
15   order to track the sun continuously over the ship, the photometer will firstly go to the sun with the last information (date, time, geolocation, heading, pitch and roll) from the GPS receiver and compass module. This can help the photometer point to the sun if the ship does not turn quickly. If the photometer does not see the sun, which can be determined through the digital number from direct sun measurements, the head will be controlled to search the sky at 45° in the left and right horizontal panels. When it detects the sun, the new position will be used to calculate the turning angle of the ship and then
20   to correct the azimuth position for next measurements. When the sun is in the tracking field of view (~ 10°), the photometer will switch into tracking mode like a regular photometer. However, what's unlike a conventional CE318-T is, the tracking mode by using the 4-quadrant detector, will keep working to compensate the motions of the ship during all the SUN triplet measurements. It is the same procedure for MOON triplet as well. ~~provide with the coordination and orientation information~~. The air pumping module generates compressed dry-clean air to the collimator to prohibit the contamination
25   of optical window by ambient sea spray. Meanwhile, we changed the wet sensor (a resistor) by an optical rain sensor to prevent the influence of the strong corrosion from the sea spray. Besides, we added an anemometer to help stop the system, because the robot itself will vibrate as wind speed increases above 45 km/h. But over the two measurement cruises, we chose the limit of 40 km/h to keep it safe.

21

The photometer arrangement is very robust and robotic to conduct 24/7 measurement without special care. The new rain sensor and anemometer worked quite well as being tested under oceanic stormy and rainy weather conditions. The collected data was finally transferred to the ~~indoor PC automatically~~ LOA server for further analysis.

This prototype has 10 channels with nominal wavelengths of 340, 380, 440, 500, 532, 670, 870, 937, 1020, 1064 nm. It can provide AOD values at nine wavelengths and PWV at both daytime and nighttime. It also has the potential of performing almucantar scanning. Further efforts and investigations would be necessary to utilise these data for aerosol microphysical research. ~~Current data was analyzed by LOA.~~ The data processing followed the same procedure described in Barreto et al. (2016). In addition, we need to save the geolocation data along with the AOD since the platform keeps moving all the time. ~~For the comparisons below, we take the level 1.5 products which are the currently available results from LOA.~~

2.2 MICROTOPS II

AOD and PWV measurements were also ~~schedualed~~ performed with a handheld MICROTOPS II (Ichoku et al., 2002; Smirnov et al., 2002) ~~in~~ from the framework of MAN, which was proceeded by SIMBIO (Sensor Intercalibration and Merger for Biological and Interdisciplinary Oceanic Studies) (Fargion et al., 2001; Knobelspiesse et al., 2004). ~~Spectral AODs are covered at five wavelengths (380, 440, 500, 675, 870nm).~~ It was calibrated before and after the cruise by NASA Goddard Space Flight Center. This type of MICROTOPS II has 5 channels at 380, 440, 675, 870 and 936 nm.

There are three data quality levels for the AOD both from shipborne CE318-T and MICROTOPS II: Level 1.0 with no cloud screening, Level 1.5 with cloud screening and Level 2.0 (Level 1.6 for shipborne CE318-T) for cloud screening and quality assurance (Smirnov et al., 2011). We used Level 2.0 (Level 1.6 for shipborne CE318-T) AOD at 380, 440, 500 and 870 nm for our analysis below and we need to point out that 500 nm AOD from MICROTOPS II database was interpolated with using the Ångström exponent. ~~In this paper, the cloud-screened and quality assured level 2.0 data of MICROTOPS II were used for the analysis.~~

2.3 Polly[XT]

The Raman polarization lidar (Polly[XT]) was continuously operated during the entire cruise. The Polly[XT] has two telescopes with diameter of 50 and 300 mm, respectively. There are 12 detection channels connected with these two telescopes, to cover the detection range from near surface to 4 km (near-range) and from 800 m to more than 10 km (far-range). It has 8 far-range channels with wavelengths at 355 nm (total: elastic signal and cross: filtered by a polarizer), 387 nm, 407 nm, 532 nm (total and cross), 607 nm and 1064 nm, 4 near-range channels with wavelengths at 355 nm, 387 nm, 532 nm and 607 nm (Engelmann et al., 2016). ~~It can measure~~ The signal can be used to retrieve the vertical profiles of volume

depolarization ratios at 355- and 532 nm, extinction coefficients at 355- and 532 nm, backscatter coefficients at 355-, 532- and 1064 nm ~~with a 30 s and 7.5 m resolution~~, which are related with aerosol bulk properties. Hence, particle depolarization ratios at 355- and 532nm and lidar ratios at 355- and 532 nm can be retrieved, which are sensitive to particle size, shape and chemistry properties (Freudenthaler et al., 2009; Baars et al., 2016). The backscatter coefficient β and extinction

5 coefficient α are good indicators for particle concentration (Ansmann and Müller, 2005). The lidar ratio S, which is the ratio of extinction and backscatter coefficient, describes the particle absorption ability (Müller et al., 2007; Groß et al., 2011a). Absorbing particles like soot and black-carbon-containing particles have a higher lidar ratio than non-absorbing sulfate aerosol particles. Ångström exponent Å (Angstrom, 1964) which describes the relationship between optical properties (backscatter, extinction) at two wavelengths can be used as an indicator for particle size (Baars et al., 2016;

10 Ansmann et al., 2002). Normally, large particles like dust particles, have a small Å (< 0.5). On the contrary, small particles like biomass combustion aerosols, most continental aerosols, have a larger Å (> 1.0) (Müller et al., 2007; Baars et al., 2016; Eck et al., 1999). ~~These intensive parameters are sensitive to particle size, shape and chemistry properties.~~ Therefore, aerosol layers with different physical and chemical properties, like marine aerosol, dust and smoke, can be characterized based on these retrieving results.

15 ~~The Polly^{XT} lidar was equipped with a near-range telescope, and the incomplete overlap zone can be suppressed to 120 m,~~ The near-range telescope can suppress the incomplete overlap zone to 120 m, which enabled us to capture the aerosol distribution and evolution inside the marine boundary layer (MBL) (Kanitz et al., 2013; Engelmann et al., 2016). In order to avoid the damage for the photon-counting detectors from strong solar radiation, the lidar system was turned off when the solar elevation angle exceeded 70° and the 407 nm channel was turned off routinely at daytime.

20 In order to calculate the AOD, Raman method (Ansmann et al., 1992) and Fernald method (Fernald et al., 1972) were utilized for nighttime and daytime measurements, respectively. Fernald method needs the assumption of lidar ratio, which is dependent on aerosol types. In our analysis, lidar ratios of 20 sr (20 and 20 sr), 50 sr (50 and 50 sr) were used for marine aerosols and dust at 355 nm (532 and 1064 nm) (Groß et al., 2011a). This would lead to an relative error of 20% for AOD, which is dependent on the deviations of lidar ratio for the aerosol layers (Kafle and Coulter, 2013; Hughes et al., 1985).

25 Raman method can achieve better accuracy, because it doesn't need the critical assumption (Ansmann et al., 1992). However, it can lead to relatively large statistical error, due to the very weak Raman signal. Therefore, in order to make the statistical error less than 15%, we accumulated the signal within 1 hour and used vertical smoothing window to increase the signal-noise-ratio (Mattis et al., 2004; Groß et al., 2011b).

2.4 Supplementary instruments and data sources

Temperature, pressure and relative humidity (RH) profiles were obtained from radiosonde ascents. The radiosondes were launched on board the RV *Polarstern* at 11:00 UTC on each day. In order to have better temporal resolved meteorological information, Global Data Assimilation System 1° resolution (GDAS1) meteorology data (Kanamitsu, 1989) was used in

5   the lidar data analysis. This data is ~~calculated~~ processed every three hours per day with a spatial resolution of 1° (latitude, longitude) by an atmospheric model provided by National Centers for Environmental Prediction (NCEP). In addition, the Hybrid Single-Particle Lagrangian Integrated Trajectory (HYSPLIT) model (Draxler, 2011) was used for backward trajectory analysis.

3 Results

10   **3.1 Validation of shipborne CE318-T**

3.1.1 Daytime validation with MICROTOPS II

The AOD measurements were conducted with MICROTOPS II, Polly[XT] and shipborne CE318-T simultaneously at daytime and with Polly[XT] and shipborne CE318-T at nighttime. ~~In Fig. 9, the latitudinal distribution of AOD at 500 nm (532 nm) from these three instruments is displayed for the data collected during the two RV *Polarstern* cruises, PS113 and PS116.~~

15   ~~In order to calculate the AOD with lidar measurements, Fernald method (Fernald et al., 1972) was used for retrieving the daytime results, in which lidar ratios of 20 sr (20 and 20 sr), 50 sr (50 and 50 sr) were used for marine aerosols and dust at 355 nm (532 and 1064 nm) (Groß et al., 2011a). The Raman method (Ansmann et al., 1990; Ansmann et al., 1992) was used to compare the nighttime results. For the height range with incomplete overlap, the extinction coefficient was considered to be constant. In both Fig. 9a and Fig. 9b, all measurements show the same trend with peak values between 0°~~

20   ~~and 20°N (Kanitz et al., 2013), which is the outflow region of Saharan dust and as well as large amount of biomass burning aerosols. For PS113, this belt was mainly filled with dust particles, because the Ångström exponent at 440-870 nm was less than 0.4. However, for PS116, the air mass in this belt showed a mixture of dust and smoke because the Ångström exponent at 440-870 nm was larger than 1 (Baars et al., 2012). This finding is corroborated by the lidar measurements and backward trajectories. The southern hemisphere contains less anthropogenic aerosols and dust. Marine aerosol dominates.~~

25   ~~Nevertheless, lofted biomass burning aerosols from Brazil at 25°S during PS113 was also captured by Polly[XT] with a layer top height of 2 km, which is not shown here.~~ In order to evaluate the reliability and data quality of the shipborne CE318-T, we ~~show~~ showed ~~a correlation~~ linear regressions between MICROTOPS II AOD and shipborne CE318-T AOD in Fig. 4. ~~Good agreement~~ Good linear relationship was found between the shipborne CE318-T and MICROTOPS II ~~AODs~~ with R[2] (coefficient of determination) of 0.988, 0.987, ~~0.993~~ 0.994 and 0.994 for ~~the 500 nm AOD~~ AODs at 380, 440, 500 and

24

870 nm and of 0.896 for the Ångström exponent ~~was found. The deviation of AOD between those two instruments increases during severe dust outbreaks but still was below 0.03.~~ The Ångström exponent is ~~quite~~ sensitive to the measurement error at clean conditions with AOD less than 0.05. Therefore the scatter in the respective correlation in Fig. 4b is acceptable.

In order to study how the AOD from these two instruments agreed with each other, we used the Bland-Altman plots (Willmott, 1982; Knobelspiesse et al., 2019; Bland and Altman, 1986) to visualize AOD difference (ΔAOD = $AOD_{CE318-T} - AOD_{MICROTOPS}$) against the AOD mean ($\overline{AOD} = (AOD_{CE318-T} + AOD_{MICROTOPS})/2$, which can clearly display the bias and system effects. We only took the data pairs with the 500 nm AOD between 0.04 and 0.2, according to the WMO criteria for traceability (WMO). Besides, we used the metric, which is the percentage of $\overline{AOD}$ that falls out of the boundary of the mean difference $\pm 1.96 \times$ the root-mean-squared AOD difference, to indicate the agreement of two measurements. If the measurement differences are normally distributed, we can use the criteria of 5% to indicate whether the agreement is good or not (Giavarina, 2015). However, our measurements failed the normality test, which stated potential systematic errors either from MICROTOPS II or from the shipborne CE318-T, but we still keep using this metric to indicate the agreement.

From Fig. 5, we found small positive bias of 0.0019, 0.0050, 0.0052 and 0.0027 for AODs at 380, 440, 500 and 870 nm compared with MICROTOPS II and the root-mean-squared AOD differences are 0.0149, 0.0128, 0.0099 and 0.0090, respectively. Based on the research from Morys et al. (2001) and Ichoku et al. (2002), the estimated uncertainties of AOD from MICROTOPS II were about 0.02 at 340 nm and decreasing to about 0.01 at 870 nm while comparing with the AERONET field instrument, which means we can only validate other instrument to this level with taking the MICROTOPS II as the reference. Besides, the falling out percentages of the AOD difference were 3.80%, 3.80%, 7.59% and 2.53%. These results stated the AODs at 380, 440 and 870 nm from the shipborne CE318-T were in good agreement with MICROTOPS II. AOD at 500 nm was a little bit worse, as the falling out percentage exceeded 5%. But as we mentioned in Sect. 2.2, the 500 nm AOD from the MICROTOPS II was interpolated from other wavelengths, we don't know how much influence it would bring. Overall, we can conclude the daytime capabilities for the shipborne CE318-T under the real marine conditions are as good as the MICROTOPS II.

3.1.2 Nighttime comparisons with Polly[XT]

This shipborne CE318-T has the capability to conduct nighttime measurement as well. This feature can help us to investigate the diurnal evolution of marine aerosols and dust layers over the ocean. However, this function is more challenging than the daytime measurement as moon tracking is much more sensitive to errors of the leveling adjustment, ~~and~~ coordination and orientation data from the compass. Therefore, we need to analyze ~~how accurate~~ the accuracy of the nighttime measurement~~s are~~. In Fig. 6, we presented the full diurnal measurements from the shipborne CE318-T, Polly[XT] and MICROTOPS II at 26 November 2018. On this day, RV *Polarstern* had just passed Cape Verde and was heading

towards Cape Town. A mixed layer of dust and pollution aerosol was observed over the whole day. This finding is corroborated by the 532 nm volume linear depolarization ratio plot in Fig. 6c and backward trajectories in Fig. 7. The backward trajectories shows that the air mass between 1 and 3 km on 26 November 2018 originated from the Saharan desert and were over Chad and Niger six days before crossing RV *Polarstern*. ~~Only the trajectories for arrival height of~~

5 ~~500 m was probably free of pollution.~~ All the backward trajectories including the ones for 500 m and 1000 m arrival height crossed the active biomass burning regions two days before arriving RV *Polarstern*. Therefore, the advected dust layer probably took up a large amount of biomass-burning aerosols over central Africa. In order to evaluate the shipborne CE318-T AOD measurements at nighttime, AOD from Polly[XT] was calculated based on the extinction coefficient retrieved with Raman method (Ansmann et al., 1992). Above 1.5 km to 6 km, the extinction coefficient was taken from far-range channel

10 result and between 0.3 and 1.5 km, the near-range retrieving results was used. Below 0.3 km, the extinction coefficient was considered to be constant, as displayed in Fig. 8b. Besides, we've checked the signal above 6 km and found no additional aerosol layers. The overall relative error of AOD with using this approach was 11-15%, according to the error analysis from (Ansmann et al., 1992; Mattis et al., 2004; Groß et al., 2011b). The time series of AOD can be found in Fig. 6a. The deviation between nighttime shipborne CE318-T and lidar observations was less than 0.03. Daytime measurements from

15 the shipborne CE318-T are also in good agreement with MICROTOPS II at 11:00 UTC with a deviation of 0.01 and 0.01 for the 500 nm AOD and the Ångström exponent respectively.

~~The mean AOD at 532 nm is 0.42 ± 0.02 between 00:00 and 07:00 UTC. The Ångström exponent at 440-870 nm increased from 0.15 to 0.40 during this period, which indicates that the fraction of large particles decreased. A similar pattern was also found for the extinction-related Ångström exponent 355-532 nm derived from lidar data (the result is not shown here).~~

20 ~~Further detailed vertical information can be found in Fig. 8. The top of the MBL was 350 m according to the radiosonde RH and temperature profiles in Fig. 8f. The particle depolarization ratios at 355 and 532 nm inside the MBL were 0.17 ± 0.09 and 0.12 ± 0.06 and the lidar ratios at 355 and 352 nm inside the MBL were 40.19 ± 7.03 sr and 44.76 ± 3.84 sr. These values are similar to those in the lofted mixed dust layer between 1.5 and 2.5 km and quite different from typical values for pure marine conditions in Sect 3.1.1. Therefore, we can conclude that the MBL was contaminated by the transported~~

25 ~~dust and smoke particles.~~

3.2 Case studies

In Fig. 9, the latitudinal distribution of AOD at 500 nm (532 nm) from these three instruments is displayed for the data collected during the two RV *Polarstern* cruises, PS113 and PS116. ~~In order to calculate the AOD with lidar measurements, Fernald method (Fernald et al., 1972) was used for retrieving the daytime results, in which lidar ratios of 20 sr (20 and 20~~

30 ~~sr), 50 sr (50 and 50 sr) were used for marine aerosols and dust at 355 nm (532 and 1064 nm) (Groß et al., 2011a). The~~

Raman method (Ansmann et al., 1990; Ansmann et al., 1992) was used to compare the nighttime results. For the height range with incomplete overlap, the extinction coefficient was considered to be constant. In both Fig. 9a and Fig. 9b, all measurements show the same trend with peak values between 0° and 20°N (Kanitz et al., 2013), which is the outflow region of Saharan dust and large amount of biomass-burning aerosols. For PS113, this belt was mainly filled with dust particles, because the Ångström exponent at 440-870 nm was less than 0.4 and AOD was over 0.5, which was typical for Saharan dust (Toledano et al., 2007; Rittmeister et al., 2017). However, for PS116, the air mass in this belt showed a mixture of dust and smoke because the Ångström exponent at 440-870 nm was larger than 1 (Baars et al., 2012). This finding is corroborated by the lidar measurements and backward trajectories as well. On the contrary, the southern hemisphere contains less anthropogenic aerosols and dust. Under most cases, marine aerosol dominates. Nevertheless, lofted biomass burning aerosols from Brazil at 25°S during PS113 was also captured by Polly[XT] with a layer top height of 2 km, which is not shown here.

In order to illustrate the aerosol vertical distribution over the Atlantic Ocean and investigate the behavior of shipborne CE318-T at different aerosol conditions, we present the results from shipborne CE318-T, lidar and MICROTOPS II observations at pure marine condition and in cases with Saharan dust outbreaks. Moreover, the full diurnal cycle of AOD observations over the Atlantic Ocean can also be recorded with the shipborne photometry. Detailed analysis was applied based on the diurnal measurements from the shipborne CE318-T and Polly[XT] lidar and daytime measurements from MICROTOPS II.

3.2.1 Marine aerosol conditions

On 23 November 2018, RV *Polarstern* was west of Western Sahara and approaching Cape Verde. Northwestern airflow and clean marine conditions prevailed. The measurements from shipborne CE318-T and lidar were shown in Fig. 10. According to the 532 nm attenuated backscatter, typical marine aerosol conditions were observed. The 532 nm volume depolarization ratio was less than 0.05 below 1.8 km, which means that the marine boundary layer was dominated by spherical sea salt particles. The backward trajectories in Fig. 11 show that the air mass was mainly carried over the ocean during the past 4 days. Furthermore, no strong aerosol layers were observed above 2 km height. The mean AOD at 532 nm from 08:30 to 11:00 UTC based on shipborne CE318-T measurements was 0.06 ± 0.01 and mean Ångström exponent at 440-870 nm was 0.26 ± 0.03, These are typical values for marine aerosols, which are dominated by coarse mode sea salt particles (Smirnov et al, 2006). The mean AOD at 532 nm and mean Ångström exponent at 440-870 nm from MICROTOPS II were 0.05 ± 0.01 and 0.20 ± 0.03, which are in good agreement with the shipborne CE318-T.

Detailed height-resolved aerosol information was displayed in Fig. 12. According to the RH profile in Fig. 12d, the marine layer reached to about 2 km height. The mean extinction coefficient was 38.5 Mm^{-1}, 27.4 Mm^{-1} and 19.2 Mm^{-1} at 355 nm,

532 nm and 1064 nm, by using Fernald method (Fernald et al., 1972) and assuming a fixed lidar ratio of 20 sr (Groß et al., 2011a). The particle depolarization ratios below 1.6 km were less than 0.02 at 355 nm and 532 nm. From 1.7 km to 2.0 km, the particle depolarization ratio increased with peak value at 355 nm (532 nm) to be 0.09 (0.08) and RH decreased to 10 % according to the GDAS1 data. These are good indicators for dried sea salt particles (Haarig et al., 2017; Bohlmann et al., 2018). When RH drops below 45 %, the spherical marine aerosol particles start to crystallize and become cubic-like in shape. These cubic dry sea salt particles will introduce a relatively strong depolarized signal and lead to the increase of particle depolarization ratio (Haarig et al., 2017).

3.2.2 Saharan dust

When the RV *Polarstern* approached Cape Verde Islands, a dust outbreak was observed from 27 May to 31 May 2018. The whole event started with a mixture of dust and smoke above the MBL. Since 30 May 2018, the layer was lofted to 1.5 km and started to be dominated by pure Saharan dust particles.

The MICROTOPS II, shipborne CE318-T and lidar measurements from 16:00 to 17:00 UTC on 30 May 2018 are displayed in Fig. 13. According Fig. 7a, the results from the shipborne CE318-T and MICROTOPS II agreed well with mean AOD of 0.66 ± 0.03 and 0.62 ± 0.02 and mean Ångström exponent at 440-870 of 0.08 ± 0.02 and 0.07 ± 0.01. Both results indicate the presence of a large amount of large dust particles. In Fig 13c, we can see a layer, located between 0.6 km to 1 km causing slightly enhanced volume depolarization ratio and a dust layer located between 1.5 and 5 km with large volume depolarization ratio. Inside the MBL, the volume depolarization ratio was quite low which indicates that the contamination caused by dust sedimentation was small.

In Fig. 14, we present the averaged vertical profiles from lidar. The extinction coefficient was retrieved by Fernald method with assuming the lidar ratios of 60 sr (355 nm), 45 sr (532 nm) and 54 sr (1064 nm) for the dust layer and 25 sr (355, 532, 1064 nm) for the MBL. The lidar ratios at 355 and 532 nm were selected based on nighttime Raman retrieving results, and the lidar ratio at 1064 nm was from AERONET measurements (Shin et al., 2018). Meanwhile, reference values were tuned to achieve the best agreement of AOD between lidar and shipborne CE318-T. Inside the MBL, the mean extinction coefficients at 355 nm and 532 nm are 245 Mm^{-1} and 241 Mm^{-1} according to Fig. 14a, which is very large compared to pure marine conditions in Sect. 3.1.1. This might be caused by the loading and hygroscopic growth of anthropogenic aerosols. This assumption is corroborated by the backward trajectories in Fig. 15a, because a branch of the backward trajectories arriving at 500 m can be traced back to European continent. The lofted dust layer extended from 1.5 to 5 km with mean extinction coefficients at 355 nm, 532 nm and 1064 nm to be 166 Mm^{-1}, 161 Mm^{-1} and 159 Mm^{-1} and particle depolarization ratios at 355 nm and 532 nm to be 0.21 ± 0.05 and 0.31 ± 0.05, which are in good agreement with optical properties for pure Saharan dust (Groß et al., 2011a; Groß et al., 2011b; Tesche et al., 2009). The backward trajectories in

28

Fig. 15b showed the air mass at 4 km originated from Chad, Libya and Sudan, and travelled 5 days from these regions before reaching RV *Polarstern*. A relatively clean layer can be found between the lofted dust layer and MBL with extinction coefficient and particle depolarization ratio less than 25 Mm^{-1} and 0.04, respectively. Therefore, we are convinced that the sedimentation of dust particles was negligible. Above the MBL, from 0.5 km to 1 km, there was an aerosol layer with

5   enhanced particle depolarization ratio at 355 nm (532 nm) of 0.11 (0.15). The backward trajectories for this layer was similar with Fig. 15a. Therefore, it probably consisted of relatively dry aged anthropogenic particles or mixture of dry aged anthropogenic particles and dry sea salt particles.

4 Conclusions

Shipborne CE318-T measurements were conducted during two trans-Atlantic RV *Polarstern* cruises together with

10   collocated Polly^{XT} lidar and independent MICROTOPS II. The shipborne CE318-T has a special design to avoid contamination of sea-spray and achieved the goal of automatic measurement over the ocean during the entire 4-5 weeks periods of the two cruises.

~~Good agreement was found between the different measurements~~ From linear regression and Bland-Altman plot, we found the capabilities of the shipborne CE318-T under the real oceanic conditions were as good as the manually operated

15   MICROTOPS II to capture the daytime AOD variabilities. For nighttime measurements, deviations between the 532 nm AOD observed with Polly^{XT} and the shipborne CE318-T was found to be less than 10 %. ~~However, we found that nighttime measurements with the shipborne CE318-T are very sensitive to errors in the leveling adjustment and the compass data, Thus, great care must be taken when setting up the system. A very good compass calibration is required as well. These issues need to be tackled or mitigated in future development.~~

20   The almucantar scanning option will also be implemented in near future, which allow the retrieval of aerosol microphysical properties over the ocean. All of these features will significantly increase our potential to characterize marine aerosol distribution over the remote ocean and the impact of continental dust, smoke, and haze outbreaks on the aerosol conditions far away from the continent, as well as dust ~~transportation~~ transport and dust sedimentation over the less exploited oceans.

instruments during PS116 and were responsible for the lidar measurements during PS116. PG, LB, GD, SV and FM built up the ~~prototype of~~ the shipborne CE318-T and were responsible for the corresponding data analysis. All authors contributed to scientific discussion and in this way to the manuscript preparation.

Competing interests. The authors declare that they have no conflict of interests.

References

Althausen, D., Engelmann, R., Baars, H., Heese, B., Ansmann, A., Müller, D., and Komppula, M.: Portable Raman lidar PollyXT for automated profiling of aerosol backscatter, extinction, and depolarization, Journal of Atmospheric and Oceanic Technology, 26, 2366-2378, https://doi.org/10.1175/2009jtecha1304.1, 2009.

Angstrom, A.: The Parameters of Atmospheric Turbidity, Tellus, 16, 64-75, https://doi.org/10.1111/j.2153-3490.1964.tb00144.x, 1964.

Ansmann, A., Riebesell, M., and Weitkamp, C.: Measurement of atmospheric aerosol extinction profiles with a Raman lidar, Opt. Lett., 15, 746-748, https://doi.org/10.1364/OL.15.000746, 1990.

Ansmann, A., Riebesell, M., Wandinger, U., Weitkamp, C., Voss, E., Lahmann, W., and Michaelis, W.: Combined Raman Elastic-Backscatter Lidar for Vertical Profiling of Moisture, Aerosol Extinction, Backscatter, and Lidar Ratio, Appl Phys B-Photo, 55, 18-28, https://doi.org/10.1007/Bf00348608, 1992.

Ansmann, A., Wagner, F., Müller, D., Althausen, D., Herber, A., von Hoyningen-Huene, W., and Wandinger, U.: European pollution outbreaks during ACE 2: Optical particle properties inferred from multiwavelength lidar and star-Sun photometry, Journal of Geophysical Research: Atmospheres, 107, AAC 8-1-AAC 8-14, https://doi.org/10.1029/2001jd001109, 2002.

Ansmann, A., and Müller, D.: Lidar and atmospheric aerosol particles, in: Lidar, Springer, 105-141, 2005.

Baars, H., Ansmann, A., Althausen, D., Engelmann, R., Heese, B., Muller, D., Artaxo, P., Paixao, M., Pauliquevis, T., and Souza, R.: Aerosol profiling with lidar in the Amazon Basin during the wet and dry season, J Geophys Res-Atmos, 117, https://doi.org/10.1029/2012jd018338, 2012.

Baars, H., Kanitz, T., Engelmann, R., Althausen, D., Heese, B., Komppula, M., Preissler, J., Tesche, M., Ansmann, A., Wandinger, U., Lim, J. H., Ahn, J. Y., Stachlewska, I. S., Amiridis, V., Marinou, E., Seifert, P., Hofer, J., Skupin, A., Schneider, F., Bohlmann, S., Foth, A., Bley, S., Pfuller, A., Giannakaki, E., Lihavainen, H., Viisanen, Y., Hooda, R. K., Pereira, S. N., Bortoli, D., Wagner, F., Mattis, I., Janicka, L., Markowicz, K. M., Achtert, P., Artaxo, P., Pauliquevis, T., Souza, R. A. F., Sharma, V. P., van Zyl, P. G., Beukes, J. P., Sun, J. Y., Rohwer, E. G., Deng, R. R., Mamouri, R. E., and Zamorano, F.: An overview of the first decade of Polly(NET): an emerging network of automated Raman-polarization lidars for continuous aerosol profiling, Atmospheric Chemistry and Physics, 16, 5111-5137, https://doi.org/10.5194/acp-16-5111-2016, 2016.

Barreto, A., Cuevas, E., Granados-Munoz, M. J., Alados-Arboledas, L., Romero, P. M., Grobner, J., Kouremeti, N., Almansa, A. F., Stone, T., Toledano, C., Roman, R., Sorokin, M., Holben, B., Canini, M., and Yela, M.: The new sun-sky-lunar Cimel CE318-T multiband photometer - a comprehensive performance evaluation, Atmospheric Measurement Techniques, 9, 631-654, https://doi.org/10.5194/amt-9-631-2016, 2016.

Bland, J. M., and Altman, D.: Statistical methods for assessing agreement between two methods of clinical measurement, The lancet, 327, 307-310, https://doi.org/10.1016/s0140-6736(86)90837-8, 1986.

Bohlmann, S., Baars, H., Radenz, M., Engelmann, R., and Macke, A.: Ship-borne aerosol profiling with lidar over the Atlantic Ocean: from pure marine conditions to complex dust-smoke mixtures, Atmospheric Chemistry and Physics, 18, 9661-9679, https://doi.org/10.5194/acp-18-9661-2018, 2018.

Draxler, R. R.: Hysplit (hybrid single-particle lagrangian integrated trajectory) model access via NOAA ARL ready website, https://ready.arl.noaa.gov/HYSPLIT.php, 2011.

Eck, T. F., Holben, B. N., Reid, J. S., Dubovik, O., Smirnov, A., O'Neill, N. T., Slutsker, I., and Kinne, S.: Wavelength dependence of the optical depth of biomass burning, urban, and desert dust aerosols, J Geophys Res-Atmos, 104, 31333-31349, https://doi.org/10.1029/1999jd900923, 1999.

Engelmann, R., Kanitz, T., Baars, H., Heese, B., Althausen, D., Skupin, A., Wandinger, U., Komppula, M., Stachlewska, I. S., Amiridis, V., Marinou, E., Mattis, I., Linne, H., and Ansmann, A.: The automated multiwavelength Raman polarization and water-vapor lidar Polly(XT): the neXT generation, Atmospheric Measurement Techniques, 9, 1767-1784, https://doi.org/10.5194/amt-9-1767-2016, 2016.

Fargion, G. S., McClain, C. R., Fukushima, H., Nicolas, J. M., and Barnes, R. A.: Ocean color instrument intercomparisons and cross-calibrations by the SIMBIOS Project, Sensors, Systems, and Next-Generation Satellites III, 1999, 397-403,

Fargion, G. S., Barnes, R., and McClain, C.: In Situ Aerosol Optical Thickness Collected by the SIMBIOS Program (1997-2000): Protocols, and and Data QC and Analysis, 2001.

Fernald, F. G., Herman, B. M., and Reagan, J. A.: Determination of aerosol height distributions by lidar, Journal of Applied meteorology, 11, 482-489, https://doi.org/10.1175/1520-0450(1972)011%3C0482:doahdb%3E2.0.co;2, 1972.

5 Freudenthaler, V., Esselborn, M., Wiegner, M., Heese, B., Tesche, M., Ansmann, A., Muller, D., Althausen, D., Wirth, M., Fix, A., Ehret, G., Knippertz, P., Toledano, C., Gasteiger, J., Garhammer, M., and Seefeldner, M.: Depolarization ratio profiling at several wavelengths in pure Saharan dust during SAMUM 2006, Tellus Series B-Chemical and Physical Meteorology, 61, 165-179, https://doi.org/10.1111/j.1600-0889.2008.00396.x, 2009.

Giavarina, D.: Understanding bland altman analysis, Biochemia medica: Biochemia medica, 25, 141-151,
10 https://doi.org/10.11613/bm.2015.015, 2015.

Goloub, P., Blarel, L., Dubios, G., Popovici, I., Podvin, T., Torres, B., Victori, S., Maupin, F., and Pikridas, M.: Current results on mobile system prototype development for Aerosol Cal/Val activities, ESA/IDEAS Project WP 3440-1/3/5, 12 Dec, 2017, 2017.

Groß, S., Tesche, M., Freudenthaler, V., Toledano, C., Wiegner, M., Ansmann, A., Althausen, D., and Seefeldner, M.:
15 Characterization of Saharan dust, marine aerosols and mixtures of biomass-burning aerosols and dust by means of multi-wavelength depolarization and Raman lidar measurements during SAMUM 2, Tellus B: Chemical and Physical Meteorology, 63, 706-724, https://doi.org/10.3402/tellusb.v63i4.16369, 2011a.

Groß, S., Wiegner, M., Freudenthaler, V., and Toledano, C.: Lidar ratio of Saharan dust over Cape Verde Islands: Assessment and error calculation, Journal of Geophysical Research: Atmospheres, 116,
20 https://doi.org/10.1029/2010JD015435, 2011b.

Haarig, M., Ansmann, A., Gasteiger, J., Kandler, K., Althausen, D., Baars, H., Radenz, M., and Farrell, D. A.: Dry versus wet marine particle optical properties: RH dependence of depolarization ratio, backscatter, and extinction from multiwavelength lidar measurements during SALTRACE, Atmospheric Chemistry and Physics, 17, 14199, https://doi.org/10.5194/acp-2017-545, 2017.

25 Hughes, H. G., Ferguson, J. A., and Stephens, D. H.: Sensitivity of a lidar inversion algorithm to parameters relating atmospheric backscatter and extinction, Applied optics, 24, 1609-1613, https://doi.org/10.1364/ao.24.001609, 1985.

Ichoku, C., Levy, R., Kaufman, Y. J., Remer, L. A., Li, R. R., Martins, V. J., Holben, B. N., Abuhassan, N., Slutsker, I., and Eck, T. F.: Analysis of the performance characteristics of the five-channel Microtops II Sun photometer for measuring aerosol optical thickness and precipitable water vapor, Journal of Geophysical Research: Atmospheres, 107, AAC 5-1-
30 AAC 5-17, https://doi.org/10.1029/2001jd001302, 2002.

Kafle, D., and Coulter, R.: Micropulse lidar-derived aerosol optical depth climatology at ARM sites worldwide, Journal of Geophysical Research: Atmospheres, 118, 7293-7308, https://doi.org/10.1002/jgrd.50536, 2013.

Kanamitsu, M.: Description of the NMC global data assimilation and forecast system, Weather and Forecasting, 4, 335-342, https://doi.org/10.1175/1520-0434(1989)004%3C0335:dotngd%3E2.0.co;2, 1989.

5   Kanitz, T.: Vertical distribution of aerosols above the Atlantic Ocean, Punta Arenas (Chile), and Stellenbosch (South Africa). Characterization, solar radiative effects and ice nucleating properties, https://doi.org/10.14279/depositonce-3386, 2012.

Kanitz, T., Ansmann, A., Engelmann, R., and Althausen, D.: North-south cross sections of the vertical aerosol distribution over the Atlantic Ocean from multiwavelength Raman/polarization lidar during Polarstern cruises, J Geophys Res Atmos,

10   118, 2643-2655, https://doi.org/10.1002/jgrd.50273, 2013.

Karol, Y., Tanré, D., Goloub, P., Vervaerde, C., Balois, J., Blarel, L., Podvin, T., Mortier, A., and Chaikovsky, A.: Airborne sun photometer PLASMA: concept, measurements, comparison of aerosol extinction vertical profile with lidar, Atmospheric Measurement Techniques, 6, 2383-2389, https://doi.org/10.5194/amt-6-2383-2013, 2013.

Knobelspiesse, K., Tan, Q., Bruegge, C., Cairns, B., Chowdhary, J., van Diedenhoven, B., Diner, D., Ferrare, R., van

15   Harten, G., and Jovanovic, V.: Intercomparison of airborne multi-angle polarimeter observations from the Polarimeter Definition Experiment, Applied optics, 58, 650-669, https://doi.org/10.1364/ao.58.000650, 2019.

Knobelspiesse, K. D., Pietras, C., Fargion, G. S., Wang, M., Frouin, R., Miller, M. A., Subramaniam, A., and Balch, W. M.: Maritime aerosol optical thickness measured by handheld sun photometers, Remote Sensing of Environment, 93, 87-106, https://doi.org/10.1016/j.rse.2004.06.018, 2004.

20   Livingston, J. M., Russell, P. B., Reid, J. S., Redemann, J., Schmid, B., Allen, D. A., Torres, O., Levy, R. C., Remer, L. A., and Holben, B. N.: Airborne Sun photometer measurements of aerosol optical depth and columnar water vapor during the Puerto Rico Dust Experiment and comparison with land, aircraft, and satellite measurements, Journal of Geophysical Research: Atmospheres, 108, 2003.

Macke, A., Kalisch, J., Zoll, Y., and Bumke, K.: Radiative effects of the cloudy atmosphere from ground and satellite based

25   observations, EPJ Web of Conferences, 2010, 83-94,

MAN: AERONET Maritime Aerosol Network database, available at: https://aeronet.gsfc.nasa.gov/new_web/maritime_aerosol_network.html. Last access: 4 February 2019,

Mattis, I., Ansmann, A., Müller, D., Wandinger, U., and Althausen, D.: Multiyear aerosol observations with dual-wavelength Raman lidar in the framework of EARLINET, Journal of Geophysical Research: Atmospheres, 109,

30   https://doi.org/10.1029/2004jd004600, 2004.

Morys, M., Mims III, F. M., Hagerup, S., Anderson, S. E., Baker, A., Kia, J., and Walkup, T.: Design, calibration, and performance of MICROTOPS II handheld ozone monitor and Sun photometer, Journal of Geophysical Research: Atmospheres, 106, 14573-14582, https://doi.org/10.1029/2001jd900103, 2001.

Müller, D., Ansmann, A., Mattis, I., Tesche, M., Wandinger, U., Althausen, D., and Pisani, G.: Aerosol-type-dependent lidar ratios observed with Raman lidar, Journal of Geophysical Research: Atmospheres, 112, https://doi.org/10.1029/2006jd008292, 2007.

Rittmeister, F., Ansmann, A., Engelmann, R., Skupin, A., Baars, H., Kanitz, T., and Kinne, S.: Profiling of Saharan dust from the Caribbean to western Africa-Part 1: Layering structures and optical properties from shipborne polarization/Raman lidar observations, Atmospheric Chemistry and Physics, 17, 12963-12983, https://doi.org/10.5194/acp-17-12963-2017, 2017.

Shin, S. K., Tesche, M., Kim, K., Kezoudi, M., Tatarov, B., Muller, D., and Noh, Y.: On the spectral depolarisation and lidar ratio of mineral dust provided in the AERONET version 3 inversion product, Atmospheric Chemistry and Physics, 18, 12735-12746, https://doi.org/10.5194/acp-18-12735-2018, 2018.

Smirnov, A., Holben, B. N., Kaufman, Y. J., Dubovik, O., Eck, T. F., Slutsker, I., Pietras, C., and Halthore, R. N.: Optical properties of atmospheric aerosol in maritime environments, Journal of the Atmospheric Sciences, 59, 501-523, 2002.

Smirnov, A., Holben, B. N., Slutsker, I., Giles, D. M., McClain, C. R., Eck, T. F., Sakerin, S. M., Macke, A., Croot, P., Zibordi, G., Quinn, P. K., Sciare, J., Kinne, S., Harvey, M., Smyth, T. J., Piketh, S., Zielinski, T., Proshutinsky, A., Goes, J. I., Nelson, N. B., Larouche, P., Radionov, V. F., Goloub, P., Moorthy, K. K., Matarrese, R., Robertson, E. J., and Jourdin, F.: Maritime Aerosol Network as a component of Aerosol Robotic Network, J Geophys Res-Atmos, 114, https://doi.org/10.1029/2008jd011257, 2009.

Smirnov, A., Holben, B. N., Giles, D. M., Slutsker, I., O'Neill, N. T., Eck, T. F., Macke, A., Croot, P., Courcoux, Y., Sakerin, S. M., Smyth, T. J., Zielinski, T., Zibordi, G., Goes, J. I., Harvey, M. J., Quinn, P. K., Nelson, N. B., Radionov, V. F., Duarte, C. M., Losno, R., Sciare, J., Voss, K. J., Kinne, S., Nalli, N. R., Joseph, E., Moorthy, K. K., Covert, D. S., Gulev, S. K., Milinevsky, G., Larouche, P., Belanger, S., Horne, E., Chin, M., Remer, L. A., Kahn, R. A., Reid, J. S., Schulz, M., Heald, C. L., Zhang, J., Lapina, K., Kleidman, R. G., Griesfeller, J., Gaitley, B. J., Tan, Q., and Diehl, T. L.: Maritime aerosol network as a component of AERONET - first results and comparison with global aerosol models and satellite retrievals, Atmospheric Measurement Techniques, 4, 583-597, https://doi.org/10.5194/amt-4-583-2011, 2011.

Stocker, T.: Climate change 2013: the physical science basis: Working Group I contribution to the Fifth assessment report of the Intergovernmental Panel on Climate Change, Cambridge University Press, 2014.

Tesche, M., Ansmann, A., Muller, D., Althausen, D., Mattis, I., Heese, B., Freudenthaler, V., Wiegner, M., Esselborn, M., Pisani, G., and Knippertz, P.: Vertical profiling of Saharan dust with Raman lidars and airborne HSRL in southern Morocco

34

during SAMUM, Tellus Series B-Chemical and Physical Meteorology, 61, 144-164, https://doi.org/10.1111/j.1600-0889.2008.00390.x, 2009.

Toledano, C., Cachorro, V., Berjon, A., De Frutos, A., Sorribas, M., De la Morena, B., and Goloub, P.: Aerosol optical depth and Ångström exponent climatology at El Arenosillo AERONET site (Huelva, Spain), Quarterly Journal of the Royal Meteorological Society: A journal of the atmospheric sciences, applied meteorology and physical oceanography, 133, 795-807, https://doi.org/10.1002/qj.54, 2007.

Willmott, C. J.: Some comments on the evaluation of model performance, Bulletin of the American Meteorological Society, 63, 1309-1313, https://doi.org/10.1175/1520-0477(1982)063%3C1309:scoteo%3E2.0.co;2, 1982.

WMO, W.: GAW Experts Workshop on a Global Surface Based Network for Long Term Observations of Column Aerosol Optical Properties, edited by U. Baltensperger, L. Barrie, C. Wehrli, GAW Report,
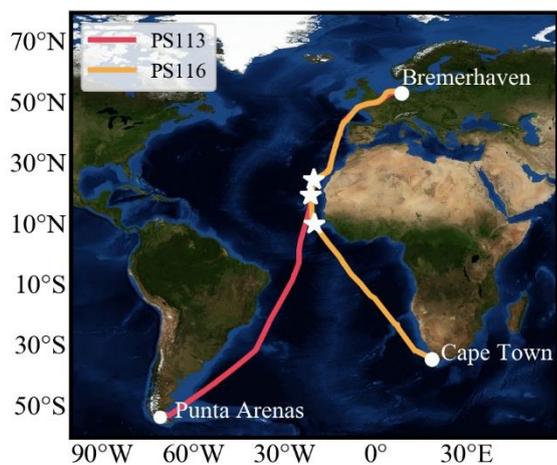
Figure 1. Ship tracks for RV *Polarstern* cruises. PS113 started from Punta Arenas, Chile on 7 May 2018 and arrived at Bremerhaven, Germany on 11 June 2018. PS116 started from Bremerhaven, Germany on 11 December 2018 and arrived at Cape Town, South Africa on 11 December 2018. White stars mark the location of the case studies presented in Sect. 3.
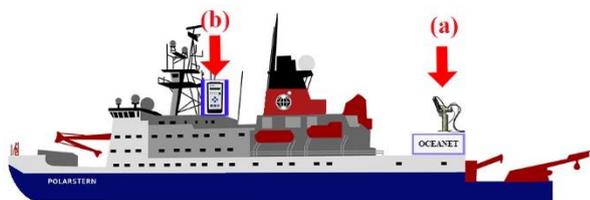
5

Figure 2 Photometer and lidar observations aboard RV *Polarstern*. MICROTOPS II observations were performed at site (b). Lidar and shipborne CE318-T observations were conducted at site (a).
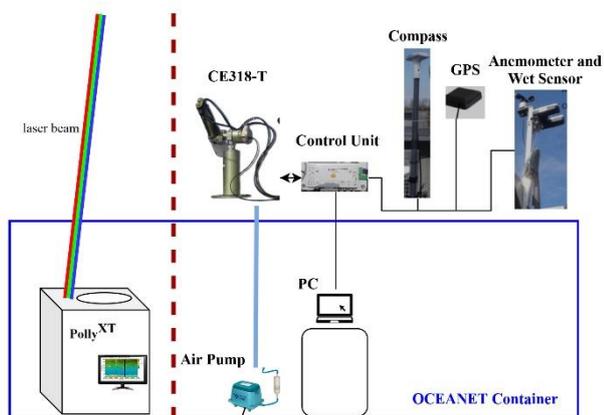
Figure 3. Sketch of the Polly^{XT} lidar (left of the dashed line) and the shipborne CE318-T (right of the dashed line).
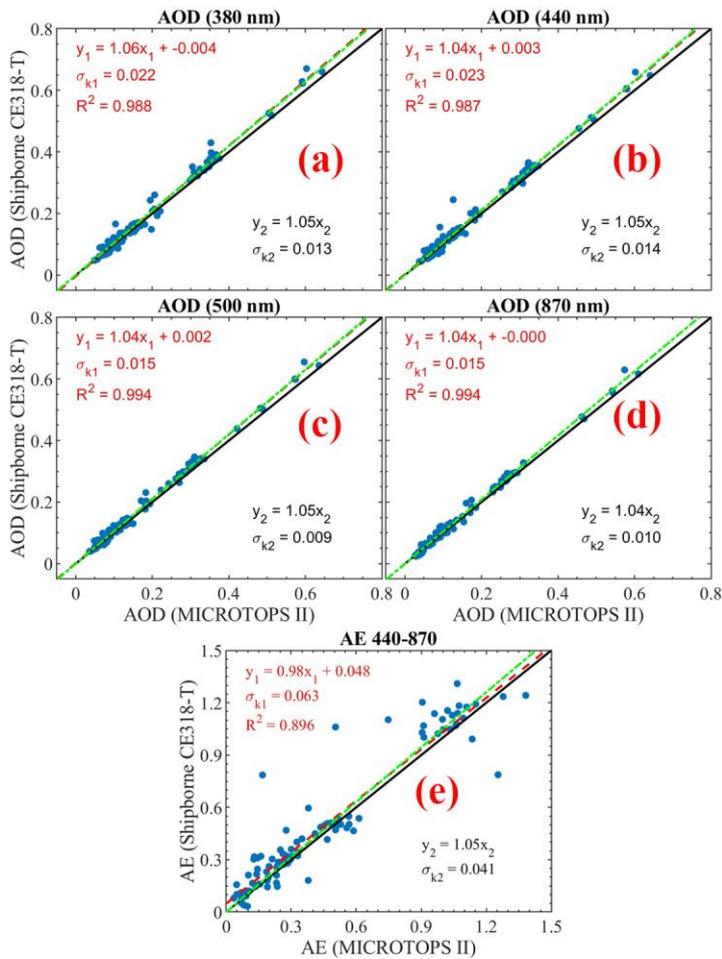
Figure 4. Linear regression of AOD (a, b, c, d) and Ångström exponent (e) from the shipborne CE318-T and MICROTOPS II observations. The data points are the mean values within a sliding window of 20 min. 115 data pairs are used in this regression. The red dashed line is the regression result with free intercept relationship and the green dot-dashed line represents the regression relationship with forced intercept through 0.

Bland-Altman plot

(a) 380 nm

(b) 440 nm

(c) 500 nm

(d) 870 nm

Mean AOD

38
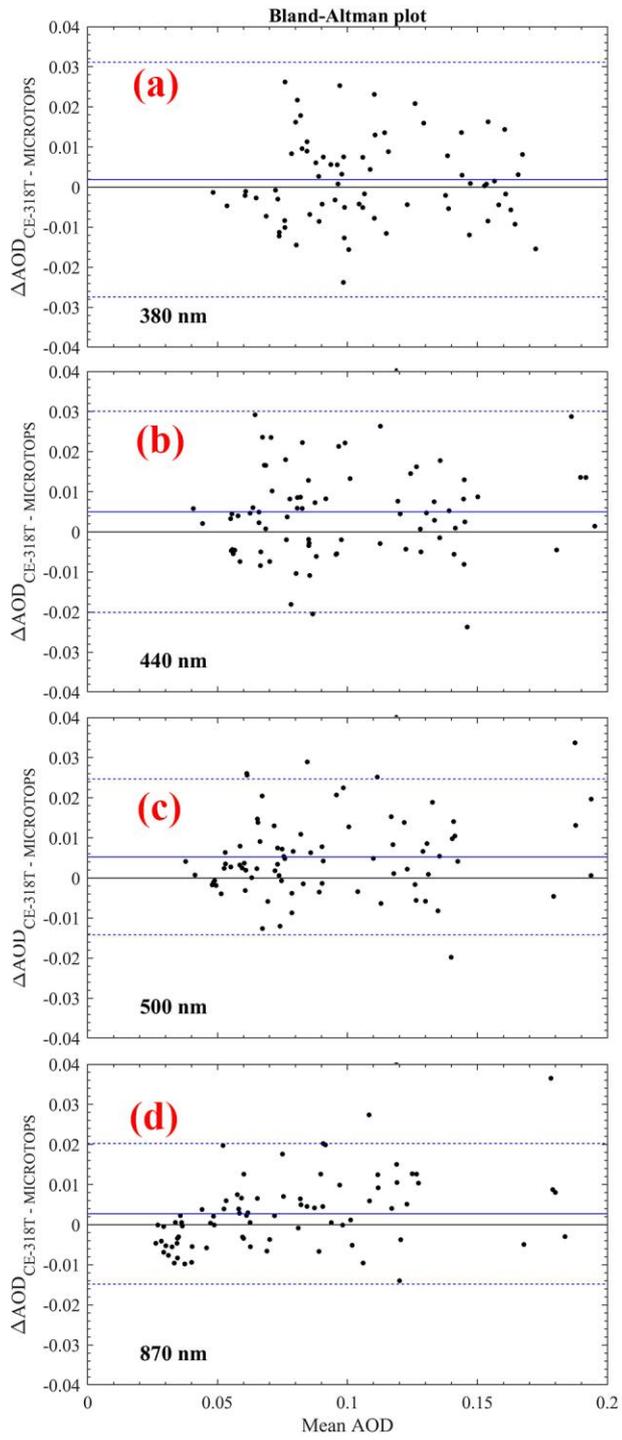
Figure 5. Bland-Altman plots for AOD differences with mean AOD (($AOD_{CE-318T}$+$AOD_{MICROTOPS}$)/2) at 380 (a), 440 (b), 500 (c) and 870 nm (d). Solid line (black) represents the 0 line. Solid line (blue) represents the mean AOD differences and dotted lines (blue) represent the mean AOD plus/minus the root-mean-squared AOD differences.
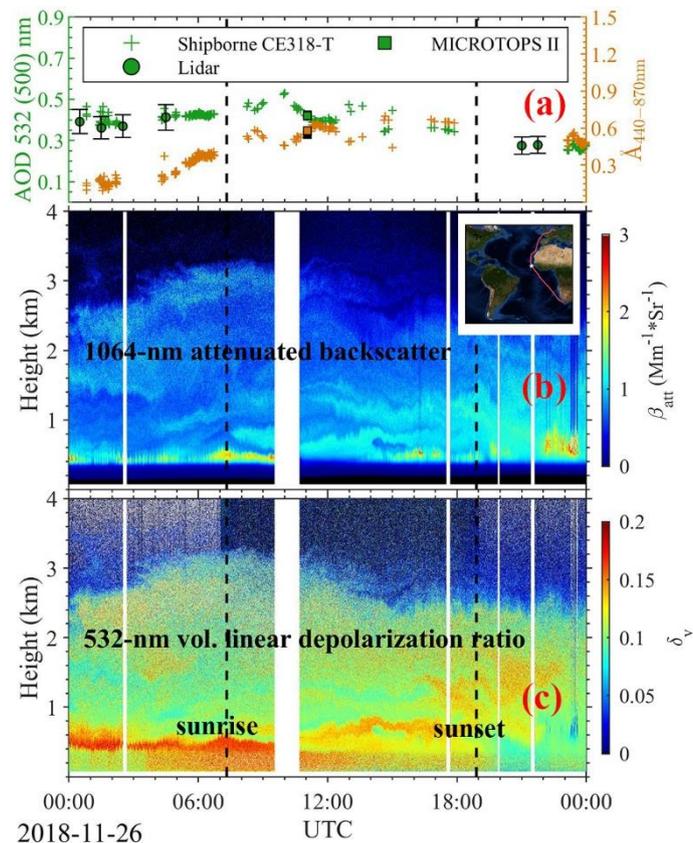
Figure 6. Shipborne aerosol observation with CE318-T, MICROTOPS II and Polly^{XT} lidar at conditions with a mixture of dust and smoke on 26 November 2018. (a) Comparison of 532 nm AOD from shipborne CE318-T and Polly^{XT} lidar observations and 500 nm AOD from MICROTOPS II measurements and Ångström exponent at 440-870 nm obtained from shipborne CE318-T and MICROTOPS II data, (b) mixed layer extended to about 3.5 km height as observed with lidar in terms of 1064 nm attenuated backscatter, and (c) volume depolarization ratio indicating dust-contaminated MBL. The narrow white strips are the lidar depolarization calibration periods and the thick white strip at 10:00 UTC is the routine turn-off time to avoid solar damage at noon.

39
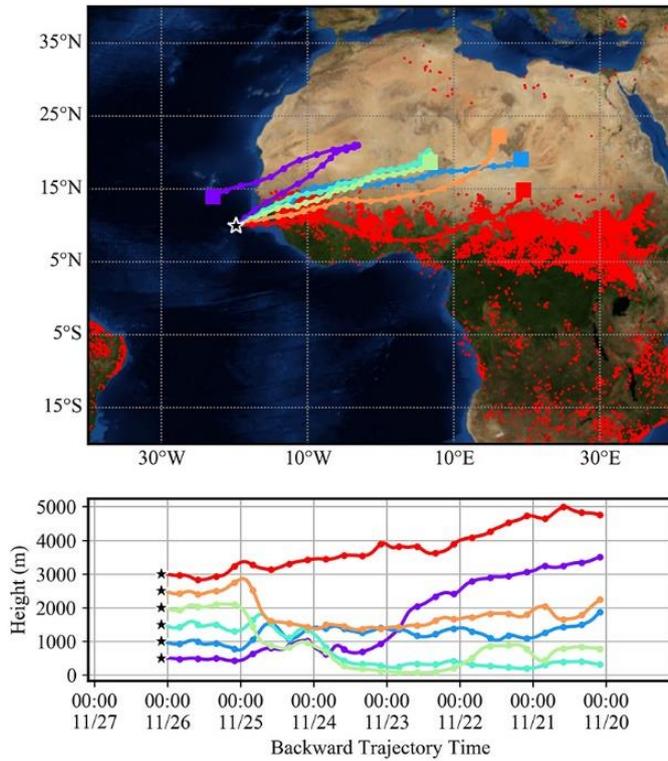
Figure 7. NOAA HYSPLIT backward trajectories arriving at RV *Polarstern* (black star with white border, 10.04 °N, 19.82 °W) on 26 November 2018, 02:00 UTC. Red dots are the fire spots detected by MODIS aboard the Terra and Aqua satellites over the period from 20 November to 26 November 2018 (last access: 4 February 2019).

5
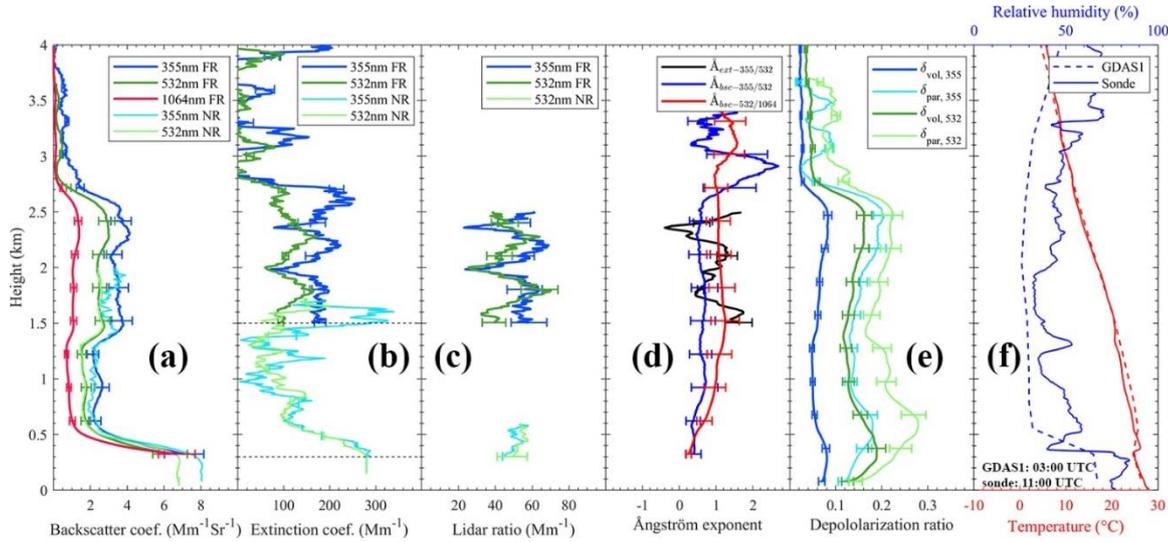
Figure 8. Raman lidar observation on 26 November 2018, 02:00-03:00 UTC. (a) Particle backscatter coefficients, (b) particle extinction coefficients (Raman lidar method), (c) lidar ratio, (d) Ångström exponents computed from different wavelengths pair in (a) and (b), (e) volume (δ_{vol}) and particle (δ_{par}) depolarization ratios, and (f) relative humidity (blue) and temperature (red) from radiosonde observations and GDAS1 dataset.
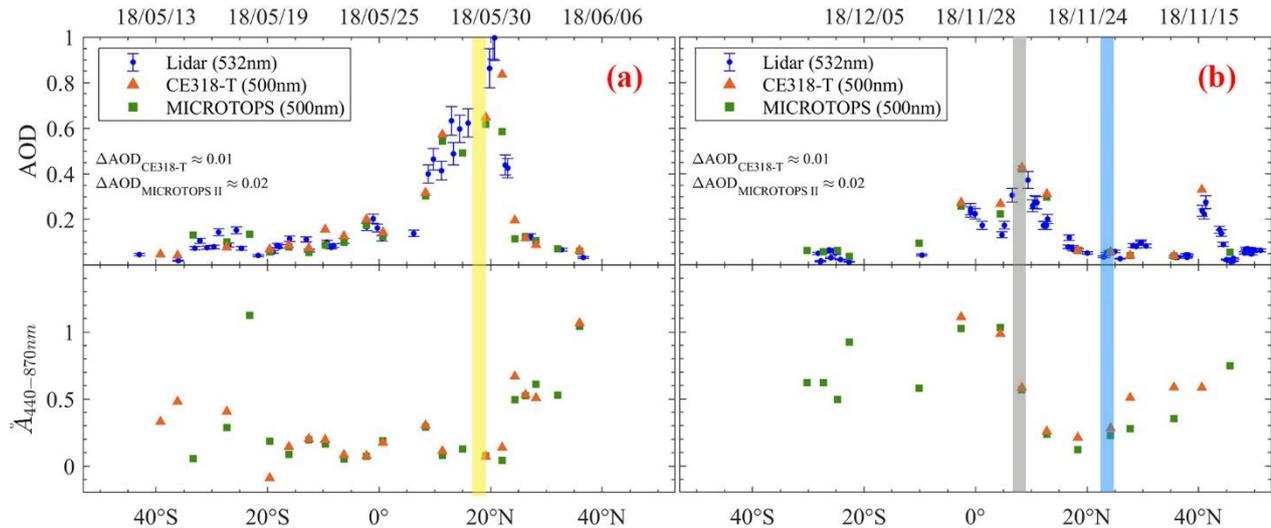
Figure 9. (a) Latitudinal distribution of daily mean AOD measured with Polly^{XT} lidar, MICROTOPS II and shipborne CE318-T. Panel (a) and (b) show the results from PS113 and PS116, respectively. The three colored vertical strips indicate the three cases used in Sect. 3.1 (yellow: Saharan dust in Fig. 13, grey: diurnal measurements in Fig. 4, ~~red~~ blue: pure marine condition in Fig. 10). Uncertainty in shipborne CE318-T and MICROTOPS II observations are referred to the analysis of Smirnov et al. (2009) and Smirnov et al. (2011).
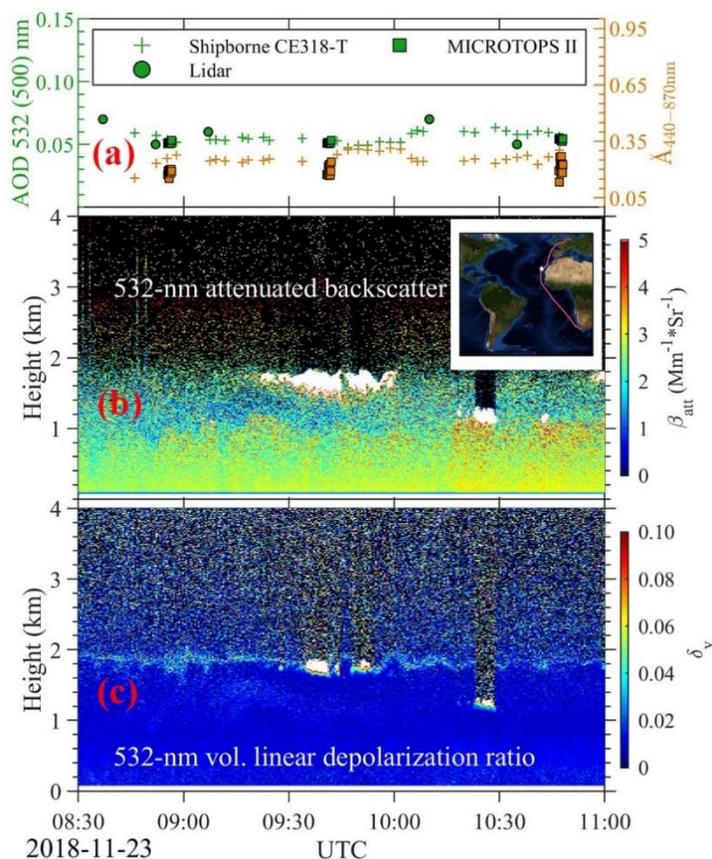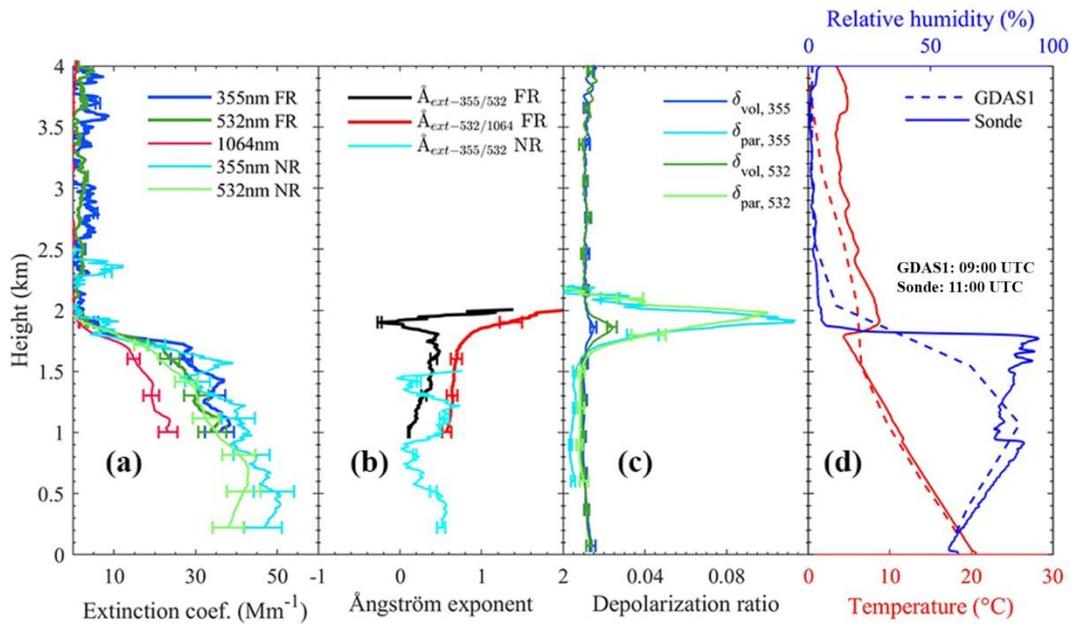
Figure 10. Shipborne aerosol observation with the shipborne CE318-T, MICROTOPS II and Polly[XT] lidar at pure marine conditions on 23 November 2018. (a) Comparison of 532 nm AOD measured with shipborne CE318-T and Polly[XT] lidar and 500 nm AOD from MICROTOPS II and Ångström exponent at 440-870 nm from shipborne CE318-T and MICROTOPS II, (b) marine aerosol layer reaching to about 2 km height, partly topped with cumulus clouds (white area), observed with lidar in terms of 532 nm attenuated backscatter, and (c) volume depolarization ratio indicating pure marine condition (very low depolarization ratio caused by the spherical droplets as sea salt particle was deliquescent at RH > 70 %) with dried cubic-like sea salt particles at the top (slightly enhanced depolarization ratio) at RH < 45 %.
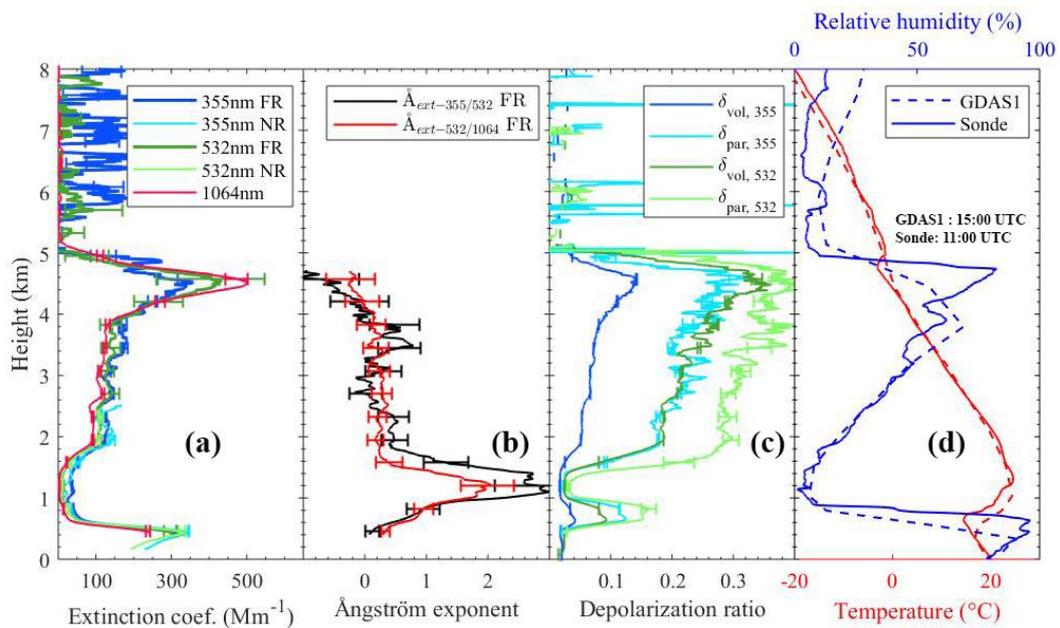
42
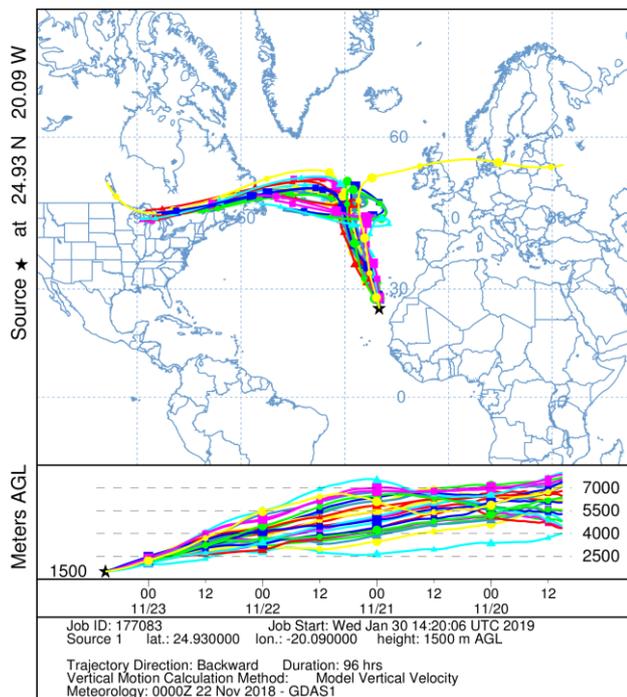
Figure 11. Six-day HYSPLIT backward trajectory ensemble arriving at 1500 m height above RV *Polarstern* (black star, 18.41 °S, 32.93 °W) on 23 November 2018, 22:00 UTC.

Figure 12 Height profiles of (a) particle extinction coefficients at 355 nm (blue, FR from far-range signal, NR from near-range signal), 532 nm (green), and 1064 nm (red), (b) Ångström exponents computed from different wavelengths pair in (a), (c) volume (δ_{vol}) and particle (δ_{par}) depolarization ratios, and (d) relative humidity (blue) and temperature (red). The lidar observations were taken on 23 November 2018, 08:30 – 09:14 UTC. The radiosonde was launched at 11:00 UTC. GDAS1 data for 09:00 UTC are shown for comparison.
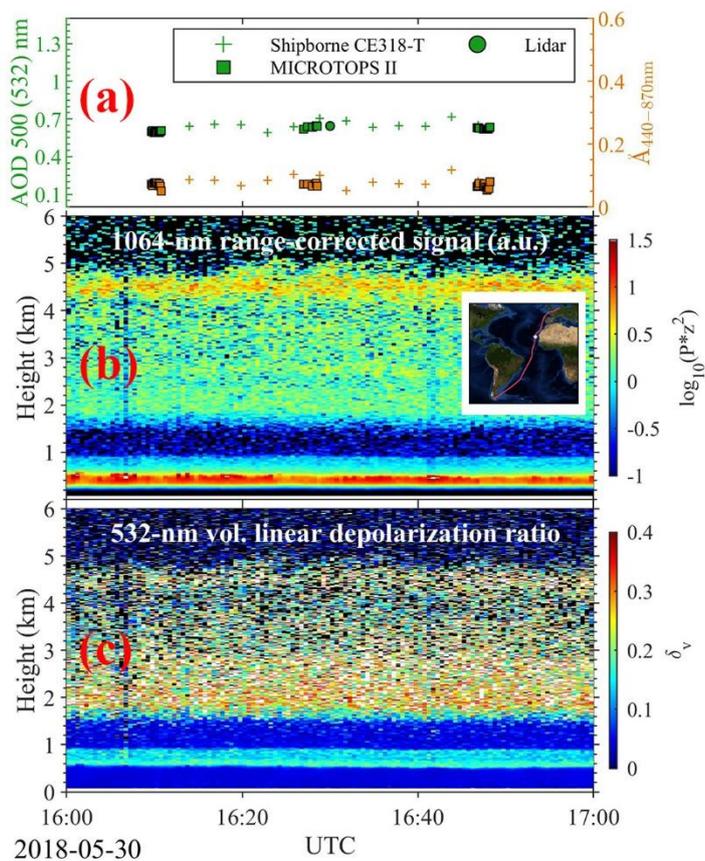
Figure 13. Shipborne aerosol observation with the shipborne CE318-T, MICROTOPS II and Polly[XT] lidar with strong dust loading on 30 May 2018. (a) Comparison of 500 nm AOD and Ångström exponent at 440-870 nm with shipborne CE318-T and MICROTOPS II, (b) the dust layer extending from 1.5 to 5 km and MBL reaching to 0.6 km, as indicated characterized by the strong range-corrected signal at 1064 nm (red), and (c) volume depolarization ratios indicating the marine layer (low values, blue) and the Saharan dust layer (high values, green and yellow).

Figure 14. Height profiles of (a) particle extinction coefficients at 355 nm (blue, FR from far-range signal, NR from near-range signal), 532 nm (green), and 1064 nm (red), (b) Ångström exponents computed from different wavelengths pair in (a), (c) volume (δ_{vol}) and particle (δ_{par}) depolarization ratios, and (d) relative humidity (blue) and temperature (red). The lidar observations were taken on 30 May 2018, 16:00 – 16:59 UTC. The radiosonde was launched at 11:00 UTC. GDAS1 data is for 15:00 UTC.
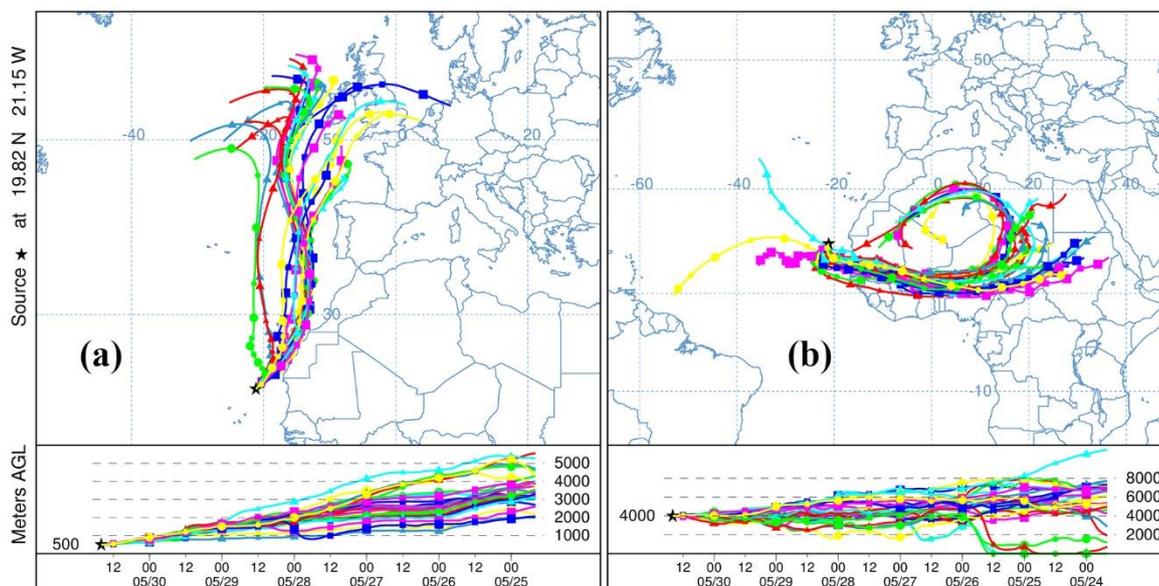
Figure 15. Six-day HYSPLIT backward trajectory ensemble arriving at 500 m (a) and 4,000 m (b) height above RV *Polarstern* (black star) on 30 May 2018, 16:00 UTC.